hydrometeorology

MDPI

Article

Urban Geoenvironmental Impact Index (UGII): A GIS-Based Fuzzy Framework Integrating Precipitation Intensity, Earth Observation and Terrain Analysis for Cumulative Environmental Susceptibility and Real-Estate Exposure Assessment

George Faidon D. Papakonstantinou

Laboratory of Physical Geography and Environmental Impacts, Department of Geography and Regional Planning, School of Rural, Surveying and Geoinformatics Engineering, National Technical University of Athens, 15780 Athens, Greece; gfpapakon@mail.ntua.gr

Abstract

Urban areas face cumulative environmental pressures from climate variability, rapid urbanization, and growing concentrations of built assets, requiring geospatial methods that capture gradual, overlapping susceptibility patterns rather than rigid thresholds. This study presents the Urban Geoenvironmental Impact Index (UGII), a GIS-based fuzzy hydro-climatic and Earth Observation (EO) framework evaluating cumulative urban environmental susceptibility and built-asset exposure, supporting hazard-informed planning and climate adaptation. Nine indicators are integrated: precipitation intensity (annualized 99th-percentile daily contribution, R99p) from ERA5-Land reanalysis (1995–2024); NDVI, NDBI, and Land Surface Temperature from Landsat 9; DEM-derived Topographic Wetness Index, flow accumulation, slope, and plan curvature; and road density. Fuzzy membership functions and AHP weighting (Consistency Ratio = 0.0537) aggregate the standardized indicators into continuous susceptibility surfaces. Applied to the southern Athens Metropolitan Area, Greece, the framework compares a conventional AHP model (UGII 0.18–0.65) with a fuzzy-AHP model (UGII 0.10–0.75; pixel-wise differences −0.09 to 0.14). The fuzzy formulation widens the dynamic range and enhances spatial differentiation while preserving the principal susceptibility patterns of the conventional model. Elevated-susceptibility zones intersect high built-asset concentrations, identifying exposure hotspots relevant to hazard-informed planning, climate adaptation, and disaster-resilience decision support, with direct application to real-estate exposure assessment.

Keywords: Urban Geoenvironmental Impact Index (UGII); cumulative environmental susceptibility; fuzzy logic; R99p (precipitation intensity); earth observation; GIS-based susceptibility assessment; AHP; real-estate planning; climate adaptation; disaster resilience

Check for updates

Academic Editor: Hanoch Lavee

Received: 17 August 2026
Revised: 12 September 2026
Accepted: 24 September 2026
Published: 21 October 2026

Copyright: © 2026 by the author. Licensee MDPI, Basel, Switzerland. This article is an open access article distributed under the terms and conditions of the Creative Commons Attribution (CC BY) license.

1. Introduction

Urban areas are increasingly shaped by the combined effects of climate variability, rapid urbanization, land-use transformation, and the continuous expansion of the built environment. These processes rarely act in isolation. Instead, they interact across space, generating complex patterns of cumulative environmental susceptibility that influence the functioning, sustainability, and resilience of contemporary metropolitan landscapes. As cities continue to grow under increasing environmental pressures, identifying where multi-

ple stressors converge has become an essential prerequisite for informed urban planning, climate adaptation, and sustainable development [1].

Urban environmental conditions emerge from the interaction of diverse natural and anthropogenic processes, including terrain morphology, hydrological dynamics, vegetation patterns, surface thermal behaviour, transportation infrastructure, and urban expansion. The combined effects of these processes cannot be adequately represented through isolated environmental indicators or single-hazard assessments. Instead, they require integrated geospatial approaches capable of combining heterogeneous spatial information into coherent susceptibility assessments that better reflect the complexity of urban systems while supporting evidence-based spatial decision-making [2].

Recent advances in Earth Observation (EO), Geographic Information Systems (GIS), and spatial modelling have substantially improved our ability to monitor environmental processes at metropolitan scales. Freely available satellite imagery, high-resolution terrain models, and open geospatial datasets now offer unprecedented opportunities to characterize urban environments with ever-increasing spatial and thematic detail. When integrated within multi-criteria analytical frameworks, these datasets enable the development of robust geospatial models capable of identifying areas where environmental pressures accumulate and interact [3,4].

Representing these interactions, however, remains a methodological challenge. Many environmental processes evolve gradually rather than through clearly defined thresholds, while their influence often changes non-linearly across space. Conventional weighted-overlay techniques and binary classifications may therefore oversimplify environmental behaviour by assuming proportional relationships between indicator values and susceptibility. Fuzzy logic serves as an effective alternative by representing environmental influence as continuous degrees of membership, allowing gradual transitions, uncertainty, and non-linear responses to be incorporated into spatial modelling. This capability is particularly valuable in urban environments, where hydrological, thermal, ecological, and anthropogenic processes interact simultaneously and continuously [5,6].

Despite considerable progress in urban geospatial analysis, many existing studies continue to focus on individual environmental processes, such as flooding, urban heat, vegetation loss, or land-use change, rather than their combined spatial interaction. Comparatively fewer studies integrate Earth Observation (EO), terrain-derived parameters, urban infrastructure, and fuzzy multi-criteria analysis within a unified framework capable of representing cumulative susceptibility while simultaneously supporting the assessment of built-asset exposure and risk-informed urban planning [7,8].

To address this gap, this study develops the Urban Geoenvironmental Impact Index (UGII) for the southern sector of the Athens Metropolitan Area, Greece. The proposed framework integrates Earth Observation-derived indicators, terrain-based morphometric and hydrological parameters, transportation infrastructure density, fuzzy membership modelling, and Analytic Hierarchy Process (AHP)-based weighting within a unified GIS environment. Rather than evaluating individual environmental processes separately, the methodology captures their cumulative spatial interactions and produces continuous susceptibility surfaces that better represent the complexity of metropolitan environments [9–11].

The proposed framework extends beyond environmental mapping by providing a transferable GIS-based decision-support tool capable of identifying areas where cumulative susceptibility coincides with high built-asset concentrations. This information supports hazard-informed urban planning, climate adaptation, infrastructure management, and real-estate exposure assessment by identifying sectors where environmental pressures are most likely to influence future urban development and redevelopment strategies [12,13].

The main contributions of this study are:

- integrating climatic (precipitation-intensity), Earth Observation, terrain-hydrological, and infrastructure indicators within a single cumulative urban susceptibility framework, coupling climatic forcing with terrain-controlled hydrological response at the metropolitan scale;
- applying fuzzy membership functions, calibrated to each indicator's observed value distribution, to represent gradual environmental transitions rather than discrete classification thresholds;
- systematically comparing conventional AHP and fuzzy-AHP formulations, including a one-at-a-time weight-sensitivity analysis demonstrating the robustness of the resulting susceptibility ranking (Spearman $\rho \geq 0.990$ under $\pm 20\%$ weight perturbation);
- integrating cumulative susceptibility with building-density data to derive a built-asset exposure surface, distinguishing areas of high environmental pressure from areas where that pressure coincides with concentrated urban development.

1.1. Urbanization, Climate Change and Urban Environmental Susceptibility

Contemporary cities are increasingly exposed to multiple environmental pressures—climatic, hydrological, and anthropogenic—that develop simultaneously and interact across space. Climate variability, rapid urbanization, expanding infrastructure, and continuous land-use transformation have altered the environmental behaviour of metropolitan areas, creating conditions where hydrological, thermal, geomorphological, ecological, and anthropogenic processes rarely operate independently. Instead, these processes reinforce one another, producing complex spatial patterns that are difficult to capture through conventional single-hazard assessments [2,14].

In this context, urban environmental susceptibility should not be interpreted as the occurrence or probability of a specific hazard. Rather, it describes the propensity of urban environments to accumulate multiple environmental pressures resulting from the interaction of natural and human-induced processes. Consequently, susceptibility represents an intrinsic characteristic of the urban landscape, reflecting how terrain configuration, hydrological behaviour, vegetation dynamics, urban sealing, infrastructure density, and surface thermal conditions combine to shape the environmental response of metropolitan systems [4,15,16].

Traditional hazard assessments commonly examine individual processes such as flooding, heat stress, erosion, or drainage-related problems. Although these approaches remain indispensable for hazard-specific investigations, they offer only a partial understanding of the environmental conditions that influence urban systems. In practice, runoff concentration, moisture accumulation, vegetation loss, surface heating, imperviousness, and infrastructure development frequently overlap, creating areas where environmental pressures exceed the influence of any single factor [17–20].

This integrated perspective is particularly relevant in Mediterranean metropolitan regions, where prolonged dry periods coexist with episodic high-intensity rainfall events, extensive urban sealing, fragmented vegetation, and rapidly expanding infrastructure within highly modified landscapes. Within the southern Athens sector, the annualized contribution of extreme daily precipitation (R99p)—derived from the 1995–2024 ERA5-Land record—ranges between 27.3–30.3 mm year^{-1}, indicating a persistent, non-negligible extreme-rainfall forcing despite the region's predominantly dry climatic regime. The resulting environmental conditions are controlled not by isolated processes but by the continuous interaction of hydrological, geomorphological, climatic, ecological, and anthropogenic drivers operating across multiple spatial scales.

Identifying areas of cumulative susceptibility provides valuable information for spatial planning and climate adaptation. Spatial susceptibility assessments can support the

prioritization of mitigation measures, guide infrastructure investments, identify environmentally sensitive urban sectors, and strengthen the integration of resilience considerations into long-term development strategies [2]. When combined with information on the spatial distribution of built assets, susceptibility mapping also provides an effective basis for evaluating environmental exposure and identifying locations where converging environmental pressures may have the greatest implications for urban development and redevelopment [21–23].

Within this perspective, cumulative urban environmental susceptibility constitutes a complementary layer of geospatial information rather than a replacement for detailed hazard-specific analyses. It provides a broader understanding of the environmental context within which individual hazards develop, offering a GIS-based spatial decision-support layer that helps integrate EO, terrain analysis, and urban infrastructure information into more comprehensive assessments of metropolitan environmental conditions [12].

1.2. Earth Observation and Urban Environmental Susceptibility Assessment

Earth Observation (EO) has fundamentally transformed the way urban environments are monitored and analysed by providing consistent, spatially explicit, and repeatedly acquired information on land-surface conditions. The increasing availability of open satellite imagery has enabled the systematic characterization of metropolitan environments at spatial scales that would be difficult, costly, or impractical to achieve through field-based surveys alone. As a result, EO has become a core component of contemporary GIS-based environmental assessment, supporting the identification of spatial patterns associated with climate adaptation, hazard assessment, and sustainable urban development [3].

Within urban environments, satellite-derived indicators capture complementary aspects of urban environmental conditions that directly influence cumulative susceptibility. Vegetation condition reflects the capacity of urban landscapes to moderate thermal stress and enhance infiltration, built-up intensity represents the degree of surface sealing and anthropogenic modification, and land surface temperature offers direct information on the spatial distribution of thermal pressure. These variables describe different but interconnected dimensions of the urban environment, each contributing to the overall geoenvironmental response of the metropolitan system [10,11,18,22].

Nevertheless, EO alone cannot fully represent the complexity of urban environmental processes. Hydrological behaviour is strongly controlled by terrain morphology, while infrastructure networks modify runoff pathways, landscape fragmentation, and patterns of urban development. Furthermore, satellite-derived indicators capture the current state of land-surface conditions but do not represent climatic forcing factors such as precipitation intensity, which operate at coarser spatial scales yet exert a direct influence on hydrological loading and runoff generation. Consequently, a comprehensive assessment of cumulative susceptibility requires the integration of EO-derived indicators with terrain-based morphometric and hydrological parameters, climatic forcing, and infrastructure-related information within a unified analytical framework [9].

In the proposed Urban Geoenvironmental Impact Index (UGII), EO therefore functions as more than merely a source of environmental variables. It forms the observational foundation upon which heterogeneous geospatial information is integrated through GIS-based multi-criteria analysis. By combining satellite-derived indicators with terrain analysis, infrastructure density, and fuzzy modelling, the framework identifies areas where multiple environmental pressures converge and interact, producing continuous susceptibility surfaces that support hazard-informed spatial planning, climate adaptation, built-asset exposure assessment, and spatial decision-making [6].

The integration of EO with GIS, fuzzy logic, and multi-criteria analysis transforms individual environmental indicators into a coherent geoenvironmental assessment framework capable of supporting evidence-based planning in rapidly evolving metropolitan environments. Rather than analysing environmental variables independently, the proposed approach reveals their cumulative spatial interactions, providing a transferable methodology that can be applied to other urban regions using widely available geospatial datasets.

1.3. Fuzzy Logic for Geoenvironmental Susceptibility Assessment

Urban environmental systems are inherently characterized by uncertainty, gradual transitions, and complex interactions among multiple environmental processes. Hydrological accumulation, terrain response, vegetation dynamics, thermal behaviour, and anthropogenic pressure rarely change abruptly across space. Instead, they evolve continuously, with their influence increasing or decreasing progressively according to local environmental conditions. Representing these gradual changes is therefore essential for realistic geoenvironmental assessment [6].

Conventional multi-criteria approaches generally rely on linear normalization or discrete classification schemes, implicitly assuming that the contribution of each environmental factor changes proportionally across its entire range of values. While these methods provide transparent and computationally efficient solutions, they may oversimplify environmental responses by imposing rigid thresholds on processes that naturally evolve in a continuous and often non-linear manner. Consequently, locations with similar environmental characteristics may be assigned substantially different susceptibility values simply because they fall on opposite sides of an arbitrary classification boundary [4,15].

Fuzzy logic offers an alternative framework by representing environmental influence as continuous degrees of membership rather than discrete classes. Instead of assuming that an environmental variable either contributes or does not contribute to susceptibility, fuzzy membership functions describe the extent to which each location belongs to a given susceptibility condition. This approach allows uncertainty, gradual transitions, and non-linear environmental responses to be incorporated directly into spatial modelling, producing susceptibility surfaces that more closely reflect the behaviour of real urban systems [6,24].

Within the proposed Urban Geoenvironmental Impact Index (UGII), fuzzy logic is employed to transform heterogeneous environmental indicators into comparable continuous susceptibility surfaces while preserving their individual environmental response patterns. Increasing sigmoidal membership functions are applied to variables positively associated with cumulative environmental susceptibility, including flow accumulation, Topographic Wetness Index (TWI), slope, concave plan curvature, Land Surface Temperature (LST), Normalized Difference Built-up Index (NDBI), precipitation intensity (R99p), and road density. Conversely, a decreasing sigmoidal function is applied to the Normalized Difference Vegetation Index (NDVI), reflecting the protective role of vegetation in moderating thermal stress, enhancing infiltration, and reducing cumulative environmental pressure [4,8,12]. For the precipitation indicator (R99p), membership function parameters were derived statistically, with the sigmoid midpoint set to the sample mean and the steepness parameter scaled to the sample standard deviation ($k = 4.394/4\sigma$, calibrated so that membership values span approximately 0.10–0.90 across ± 2 standard deviations of the observed distribution), ensuring the transformation reflects the empirical range of this variable directly. For the remaining eight indicators, midpoint and steepness parameters were calibrated based on the observed value range of each variable within the study area, informed by expert interpretation of physically meaningful transitions in each geoenvironmental process (Section 3.3.2); this calibration approach follows established practice in fuzzy-AHP susceptibility modelling [4].

Rather than replacing conventional multi-criteria analysis, fuzzy logic complements it by improving the representation of gradual environmental transitions while preserving the transparency of the weighting procedure. Combined with Analytic Hierarchy Process (AHP), the proposed fuzzy-AHP formulation retains the expert-driven weighting structure but introduces a more realistic representation of environmental processes, allowing the UGII to capture cumulative geoenvironmental impacts more effectively and deliver stronger support for hazard-informed spatial planning, climate adaptation, and built-asset exposure assessment.

1.4. Research Gap

Recent advances in EO, Geographic Information Systems (GIS), and spatial multi-criteria analysis have substantially improved the assessment of urban environmental conditions. Numerous studies have successfully mapped individual phenomena such as urban heat, flood susceptibility, vegetation loss, surface runoff, or land-use change, demonstrating the value of geospatial technologies for monitoring environmental processes at metropolitan scales. Despite these advances, most existing approaches continue to examine environmental processes separately, providing only a partial representation of the complex interactions that characterize contemporary urban environments [17,18].

Urban environmental conditions rarely result from a single controlling factor. Instead, they emerge through the combined interaction of hydrological, geomorphological, thermal, ecological, and anthropogenic processes that evolve simultaneously across space. Consequently, evaluating individual hazards independently may overlook areas where multiple environmental pressures converge, producing cumulative impacts that are not readily identified through conventional single-process assessments.

A second methodological limitation concerns the representation of environmental behaviour. Many existing GIS-based susceptibility models rely on linear normalization procedures or discrete classification schemes that assume proportional relationships between environmental variables and susceptibility. However, environmental processes frequently evolve through gradual transitions and non-linear responses, making it difficult for conventional approaches to adequately represent uncertainty and intermediate environmental conditions [4,15,24].

A further limitation is the limited integration of cumulative susceptibility with the spatial distribution of built assets. Although environmental susceptibility mapping has advanced considerably, relatively few studies explicitly connect susceptibility information with the spatial concentration of urban development to evaluate built-asset exposure. As a result, environmental assessments and urban development analyses often remain disconnected, despite the increasing importance of integrating environmental information into redevelopment strategies, infrastructure planning, climate adaptation, and long-term urban resilience [13,23].

Finally, there remains a need for transparent and transferable GIS-based frameworks that combine EO, terrain analysis, fuzzy modelling, and multi-criteria decision analysis within a unified methodology capable of supporting both cumulative susceptibility assessment and exposure-oriented spatial decision-making. Comparative evaluations between conventional weighted-overlay techniques and uncertainty-aware fuzzy approaches are still relatively limited, particularly within densely urbanized metropolitan environments where multiple environmental pressures interact simultaneously [25].

To address these methodological gaps, this study develops the Urban Geoenvironmental Impact Index (UGII), a GIS-based framework that integrates EO-derived indicators, terrain-based morphometric and hydrological parameters, transportation infrastructure density, fuzzy membership modelling, and Analytic Hierarchy Process (AHP)-based

weighting within a unified spatial assessment methodology. By combining cumulative environmental susceptibility modelling with built-asset exposure assessment, the proposed framework establishes a transferable decision-support tool for hazard-informed urban planning, climate adaptation, and sustainable metropolitan development.

1.5. Aim and Contributions

The Urban Geoenvironmental Impact Index (UGII) is proposed as a GIS-based framework for assessing cumulative urban environmental susceptibility through the integration of EO, terrain analysis, fuzzy logic, and multi-criteria decision analysis. The framework is developed and demonstrated in the southern sector of the Athens Metropolitan Area, Greece, a rapidly evolving Mediterranean metropolitan environment where hydrological, thermal, geomorphological, ecological, and anthropogenic processes interact across a highly urbanized landscape.

Rather than evaluating individual environmental processes independently, the proposed methodology captures their cumulative spatial interaction and produces continuous susceptibility surfaces that better represent the complexity of urban environmental systems. The framework further extends susceptibility assessment by integrating built-asset distribution, providing the basis for built-asset exposure assessment, supporting real-estate decision-making and hazard-informed urban planning.

The specific objectives of this study are:

- to derive complementary environmental and urban indicators from Landsat 9 imagery, Digital Elevation Model (DEM) analysis, and OpenStreetMap infrastructure data;
- to represent the environmental behaviour of these indicators through fuzzy membership functions that capture gradual transitions and non-linear responses;
- to integrate the standardized indicators using Analytic Hierarchy Process (AHP)-based weighting and compare conventional and fuzzy-AHP susceptibility modelling approaches;
- to identify urban sectors where cumulative environmental susceptibility coincides with concentrated built assets, supporting real-estate exposure assessment and spatial decision-making.

The principal scientific contributions of the proposed framework are as follows.

First, the study introduces an integrated GIS-based methodology that combines EO-derived indicators, terrain-based morphometric and hydrological variables, infrastructure density, fuzzy logic, and multi-criteria analysis within a single cumulative geoenvironmental assessment framework.

Second, it demonstrates how fuzzy membership modelling can represent gradual environmental transitions and uncertainty while preserving the transparency and interpretability of conventional AHP-based weighting.

Third, it extends cumulative environmental susceptibility assessment beyond environmental mapping by explicitly incorporating built-asset distribution to identify areas of increased environmental exposure.

Finally, the proposed methodology constitutes a transparent and transferable decision-support framework that can support hazard-informed urban planning, climate adaptation, infrastructure management, and real-estate exposure assessment in metropolitan areas undergoing environmental and urban transformation using widely available geospatial datasets. In the context of the proposed framework, the term “impact” does not denote observed environmental damage or the occurrence of a specific hazard. Instead, it refers to the cumulative geoenvironmental impact potential emerging from the spatial interaction of multiple environmental drivers, as represented through continuous susceptibility modelling. Accordingly, the UGII quantifies the spatial propensity of urban environments

to accumulate interacting environmental pressures rather than predicting individual hazardous events or their consequences.

Within the scope of this study, the term "real-estate exposure assessment" refers to the spatial evaluation of the exposure of built assets to cumulative geoenvironmental susceptibility. It does not encompass property valuation, market forecasting, or economic appraisal, but provides spatial decision-support information relevant to real-estate planning and management.

2. Study Area

The study area comprises the southern sector of the Athens Metropolitan Area (Attica Region, Greece), extending along the coastal urban front of the Saronic Gulf and including the densely urbanized municipalities of the southern suburban zone. The area includes some of the most rapidly redeveloping sectors of the Athens Metropolitan Area, including the coastal municipalities and the Ellinikon redevelopment zone.

Geomorphologically, the study area forms part of the broader Athens Basin, a low-relief metropolitan depression bounded by mountainous systems, including Mount Hymettus to the east and the Saronic coastal zone to the southwest. Elevation ranges from sea level along the coastal front to higher terrain sectors toward the northeastern margins. The terrain is dominated by relatively low-gradient urbanized surfaces interrupted by local hillslopes, runoff pathways, drainage corridors, and anthropogenically modified terrain [26,27].

The region features a Mediterranean climatic regime with hot and dry summers, mild winters, and strong seasonal thermal contrasts. In recent decades, the southern Athens sector has experienced intensified urban heat island effects, increasing surface temperatures, progressive reduction in vegetated surfaces, expansion of impervious urban cover, and increasing environmental stress associated with dense metropolitan development. Simultaneously, episodic high-intensity rainfall events combined with altered hydrological pathways and extensive urban sealing have contributed to increased runoff concentration and localized urban flooding phenomena [28–30].

The study area constitutes a well-suited environment for the application of the proposed UGII framework due to the strong spatial interaction between:

- thermal stress conditions;
- hydrological accumulation processes;
- terrain-controlled runoff dynamics;
- built-up surface concentration;
- transportation infrastructure density;
- vegetation fragmentation;
- anthropogenic landscape transformation.

The urban structure of the southern suburbs consists of heterogeneous land-use patterns including residential zones, transportation corridors, commercial districts, coastal infrastructure, recreational facilities, fragmented urban green spaces, and rapidly developing waterfront sectors. This spatial heterogeneity creates an ideal testing environment for evaluating integrated GIS-based susceptibility assessment and the spatial interaction between environmental conditions and built-asset exposure.

For the purposes of this study, Landsat 9 multispectral imagery and 30 m spatial resolution digital elevation data were utilized to derive environmental, thermal, hydrological, and morphometric indicators associated with urban environmental susceptibility. Additional urban infrastructure information was extracted from OpenStreetMap road-network data. Spatial analysis and geospatial modelling were conducted within a Geographic Information

Systems (GIS) environment using projected coordinate reference systems appropriate for regional-scale spatial analysis.

The study area was selected as the case study because it represents a characteristic Mediterranean metropolitan coastal environment where climatic stress, morphometric/terrain-hydrological processes, and urban infrastructure pressures strongly interact, producing increasingly heterogeneous spatial patterns of cumulative urban environmental susceptibility and geospatial exposure.

2.1. Athens Metropolitan Area

The study area comprises seven municipalities in the southern sector of the Athens Metropolitan Area, Greece—including Vyronas, Ilioupoli, Agios Dimitrios, Alimos, Elliniko-Argyroupoli, Glyfada, and Vari-Voula-Vouliagmeni—covering approximately 104.3 km^2 (approximately 12.3 km east–west and 22.5 km north–south). The study area extends between 37.765–37.964° N and 23.695–23.841° E. Approximately 46.6% of the study area exhibits a raw Normalized Difference Built-up Index (NDBI) exceeding zero—the standard built-up threshold [10]—confirming a densely urbanized Mediterranean environment. The study area also encompasses The Ellinikon redevelopment (Elliniko-Argyroupoli), Europe's largest ongoing urban regeneration project, spanning approximately 6.2 million m^2 (620 ha) with an estimated investment of €8 billion, providing a quantitatively substantial and practically significant case for evaluating the intersection of cumulative environmental susceptibility with concentrated built-asset redevelopment.

The southern sector of the Athens Metropolitan Area forms part of the broader Athens Basin and extends along the coastal front of the Saronic Gulf (Figure 1). The area features a continuous coastal-to-inland gradient comprising densely developed neighbourhoods, major transportation corridors, recreational areas, fragmented urban green spaces, and rapidly evolving waterfront districts. Together, these landscape characteristics strongly influence drainage organization, surface runoff, and local environmental variability, providing the physical basis for cumulative geoenvironmental assessment. This coastal-to-metropolitan gradient generates pronounced environmental and urban development contrasts, making the area particularly well suited for investigating the spatial relationship between cumulative environmental susceptibility and built-asset concentration.



Figure 1. Location of the study area within the Athens Metropolitan Area (base map: Google Earth; map data © Google; data: SIO, NOAA, U.S. Navy, NGA, GEBCO; imagery: Landsat/Copernicus, accessed September 2025).

The broader Athens Metropolitan Area occupies a basin-shaped landscape surrounded by mountainous terrain. Within the southern sector, elevation gradually increases from the coastal zone toward the eastern and northeastern margins under the influence of Mount Hymettus. Although elevation differences remain relatively moderate across much of the coastal plain, they become progressively more pronounced toward inland and peri-urban areas. This topographic configuration creates a heterogeneous terrain where low-gradient surfaces, localized slopes, and convergent drainage pathways coexist within a highly modified urban environment, influencing hydrological response and the spatial distribution of environmental processes.

The coastal setting introduces an additional dimension of environmental complexity. Shoreline features, marinas, transportation infrastructure, and adjacent urban development create a dynamic interface between coastal and inland processes. The coexistence of low-lying coastal sectors and progressively elevated inland terrain generates considerable spatial variability in runoff concentration, terrain-controlled flow pathways, surface thermal behaviour, and urban environmental conditions. This combination of natural and anthropogenic characteristics provides a suitable setting for evaluating the proposed Urban Geoenvironmental Impact Index (UGII) within a complex metropolitan environment.

2.2. Urban Development Dynamics

The southern sector of the Athens Metropolitan Area has undergone substantial urban transformation during recent decades. Residential expansion, infrastructure development, transportation network densification, coastal redevelopment, and evolving land-use patterns have progressively reshaped the spatial structure of the area. The resulting metropolitan landscape is dominated by a dense and heterogeneous built environment extending from the inland suburban zone to the Saronic Gulf coastline.

These contrasting development patterns create pronounced environmental gradients that can be effectively characterized through EO-derived indicators and GIS-based susceptibility assessment. Urban morphology changes considerably over short spatial distances, generating strong contrasts between densely built-up districts, lower-density residential areas, open spaces, and coastal infrastructure. This spatial heterogeneity provides an appropriate setting for evaluating the interaction of multiple environmental drivers within a unified geoenvironmental assessment framework.

Transportation infrastructure has played a central role in shaping the spatial organization of the southern metropolitan sector. The road network connects residential districts, commercial centres, coastal zones, and major transportation corridors while simultaneously contributing to the concentration of impervious surfaces and the modification of local environmental conditions. Consequently, road density represents an effective indicator of anthropogenic pressure and urban structural intensity within the study area.

The coastal zone is undergoing an additional phase of transformation associated with major urban regeneration initiatives, most notably the redevelopment of the former Ellinikon airport site. This large-scale project is expected to increase development intensity, investment activity, and built-asset concentration within the southern metropolitan sector, further emphasizing the importance of integrating geoenvironmental assessment into long-term planning, redevelopment strategies, and climate adaptation.

The coexistence of mature urban districts and rapidly evolving redevelopment zones makes the southern Athens sector particularly suitable for examining the relationship between cumulative environmental susceptibility and built-asset exposure. Within this context, the proposed Urban Geoenvironmental Impact Index (UGII) is applied as a GIS-based assessment approach to identify spatial variations in geoenvironmental conditions

and evaluate how these variations intersect with the spatial distribution of built assets across a dynamic metropolitan landscape.

2.3. Urban Geoenvironmental Challenges

The southern sector of the Athens Metropolitan Area is influenced by multiple interacting environmental pressures operating across a densely urbanized coastal landscape. The study area combines low-lying coastal zones, progressively elevated inland sectors, dense infrastructure networks, fragmented green spaces, and highly modified drainage systems. Together, these characteristics generate heterogeneous patterns of environmental susceptibility that cannot be adequately explained by any single environmental factor.

Hydrological processes represent one of the principal controls on the geoenvironmental dynamics of the study area. Urban development alters natural runoff pathways through surface sealing, road construction, drainage modification, and the progressive reduction in permeable land. During intense rainfall events, these changes accelerate runoff generation and concentrate surface flow within low-gradient areas, drainage corridors, and topographically convergent sectors. Consequently, Flow Accumulation and the Topographic Wetness Index (TWI) are incorporated to identify locations where terrain configuration promotes the concentration or persistence of surface water.

Terrain morphology forms an additional level of environmental control. Slope regulates runoff velocity and the downslope transfer of water, whereas concave plan curvature enhances localized flow convergence and moisture accumulation. Although these morphometric parameters do not independently determine environmental susceptibility, they strongly influence the spatial organization and intensity of hydrological processes across the metropolitan landscape.

Thermal conditions constitute a second major dimension of the urban geoenvironment. Artificial surfaces, limited vegetation cover, and dense urban fabric contribute to elevated land surface temperatures and the formation of localized thermal hotspots. These conditions vary considerably according to surface materials, development intensity, vegetation distribution, and land-use configuration. Land Surface Temperature (LST) is therefore incorporated as a direct indicator of the spatial distribution of thermal pressure.

Anthropogenic transformation further modifies the functioning of urban environmental systems. Road network density provides complementary information on urban sealing, infrastructure concentration, and the alteration of natural surface processes. The Normalized Difference Built-up Index (NDBI) characterizes the spatial distribution of built-up surfaces, whereas road density reflects neighbourhood-scale infrastructure intensity and its influence on runoff routing and landscape fragmentation. Conversely, the Normalized Difference Vegetation Index (NDVI) represents the mitigating role of vegetation by enhancing infiltration, moderating thermal conditions, and increasing the environmental buffering capacity of urban landscapes.

Collectively, these hydrological, geomorphological, thermal, ecological, and anthropogenic dimensions form the conceptual basis of the proposed Urban Geoenvironmental Impact Index (UGII). Their integration within a unified GIS-based methodology enables the identification of urban sectors where multiple environmental pressures interact, providing the basis for evaluating cumulative environmental susceptibility and its relationship with built-asset exposure.

3. Materials and Methods

The proposed Urban Geoenvironmental Impact Index (UGII) was developed as a GIS-based methodology for assessing cumulative urban environmental susceptibility in the southern sector of the Athens Metropolitan Area. The framework integrates EO-

derived indicators, terrain-based morphometric and hydrological variables, and urban infrastructure information within a GIS-based multi-criteria assessment workflow.

The methodological workflow comprises five sequential stages (Figure 2).

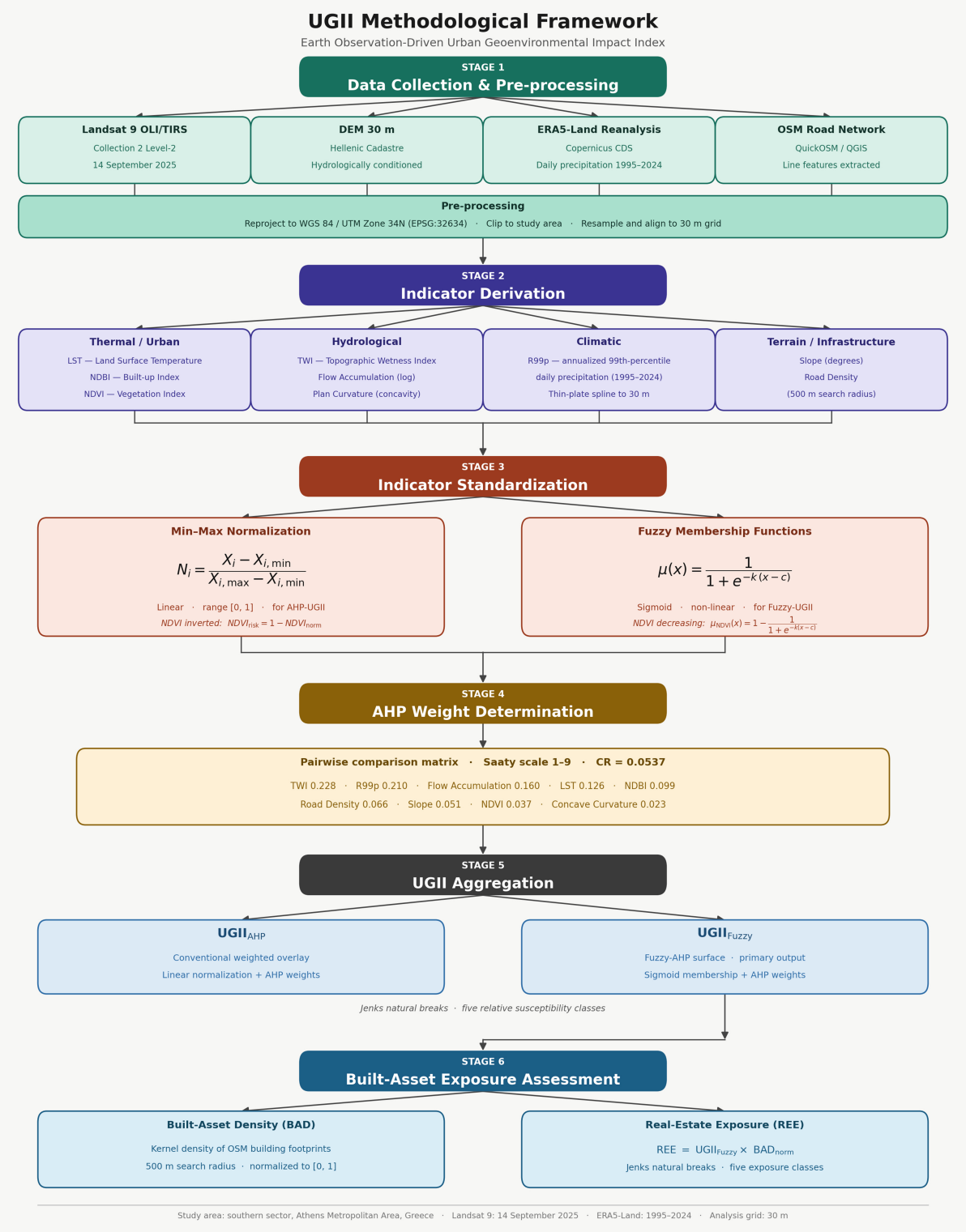


Figure 2. Overall methodological workflow of the proposed UGII framework.

First, the spatial datasets were collected, pre-processed, and harmonized within a common projected coordinate reference system. Second, geoenvironmental and urban indicators were derived from Landsat 9 imagery, Digital Elevation Model (DEM), and OpenStreetMap road-network data. Third, the resulting raster layers were standardized

using both conventional linear normalization and non-linear fuzzy membership functions. Fourth, the relative importance of the selected indicators was determined through the Analytic Hierarchy Process (AHP). Finally, the standardized indicators were aggregated to generate two complementary UGII surfaces: a conventional AHP-based model and a fuzzy-AHP model.

The comparison between the two formulations enables the evaluation of how uncertainty-aware fuzzy standardization influences the spatial distribution, and intensity of cumulative environmental susceptibility patterns. The resulting UGII surfaces serve as the basis for evaluating the built environment and built-asset exposure.

The methodological workflow is organized as follows.

3.1. Data Sources

The construction of the Urban Geoenvironmental Impact Index (UGII) was based on three primary open-access geospatial datasets: Landsat 9 Collection 2 Level-2 imagery, a 30 m spatial-resolution Digital Elevation Model (DEM), and OpenStreetMap road-network data extracted through the QuickOSM plugin in QGIS. The selected datasets provide complementary geoenvironmental information on surface thermal conditions, vegetation distribution, built-up intensity, terrain morphology, hydrological accumulation, and anthropogenic infrastructure pressure (Table 1).

Table 1. Datasets used for the construction of the Urban Geoenvironmental Impact Index.

Dataset	Source	Spatial Resolution	Derived Indicators	Analytical Role
ERA5-Land Reanalysis (daily total precipitation, 1995–2024)	Copernicus Climate Data Store (CDS)	0.1° (~9–11 km), interpolated to 30 m	R99p (annualized 99th-percentile daily precipitation contribution)	Extreme precipitation intensity and climatic hydrological forcing
Landsat 9 Collection 2 Level-2 OLI/TIRS imagery	U.S. Geological Survey—Earth Explorer	30 m	NDVI, NDBI, LST	Vegetation condition, built-up intensity, and surface thermal response
Digital Elevation Model (DEM)	Hellenic Cadastre	30 m	Flow accumulation, TWI, slope, concave plan curvature	Hydrological accumulation and terrain morphology
OpenStreetMap road network	OpenStreetMap, extracted through QuickOSM	Vector line features; rasterized density surface at 30 m	Road density within a 500 m search radius	Neighbourhood-scale infrastructure concentration and anthropogenic pressure

A Landsat 9 OLI/TIRS scene acquired on 14 September 2025 was used to derive the remotely sensed indicators. The selected Level-2 product corresponds to WRS Path 183 and Row 34. The mid-September acquisition was selected deliberately to represent late-summer environmental conditions rather than opportunistically based on data availability: a late-summer, early-afternoon overpass over an eastern-Mediterranean metropolitan area captures the seasonal maximum of thermal and hydrological stress—peak land-surface temperature and urban-heat-island expression, minimum soil moisture, and the strongest contrast between sealed and vegetated surfaces. The scene therefore represents a conservative, high-stress environmental configuration of the thermal and runoff-related pressures the index is designed to detect, while also satisfying near-cloud-free conditions over the study area (5% scene cloud cover per USGS metadata). Landsat 9 Collection 2 Level-2 products are delivered with standard atmospheric correction applied by USGS—surface reflectance via the Land Surface Reflectance Code (LaSRC) algorithm and surface temperature via the single-channel algorithm—and no additional atmospheric correction was applied. No cloud-masking artifacts were observed in the derived NDVI, NDBI, or LST layers within the study-area extent. Surface-reflectance bands were used to derive the Normalized Differ-

ence Vegetation Index (NDVI) and the Normalized Difference Built-up Index (NDBI). The Level-2 Surface Temperature product (ST_B10) was converted to degrees Celsius and used to represent Land Surface Temperature (LST).

Among the nine indicators, only LST and NDVI are sensitive to the acquisition date; the precipitation indicator (R99p) is derived from a 30-year climatological record and is therefore also time-invariant; NDBI is relatively stable at the intra-annual scale, and the terrain-derived and infrastructure layers are time-invariant. The two date-dependent indicators jointly account for approximately 16.3% of the aggregate AHP weight (LST = 0.126; NDVI = 0.037), whereas roughly 83.7% of the index is governed by temporally stable terrain, hydrological, and infrastructural components. The framework is therefore predominantly structural in nature, and its principal susceptibility patterns are largely insensitive to the choice of a single EO epoch.

Terrain-related indicators were derived from a 30 m spatial-resolution DEM. Prior to hydrological analysis, depressions were filled to obtain a hydrologically conditioned elevation surface. The processed DEM was subsequently used to calculate flow accumulation, the Topographic Wetness Index (TWI), slope, and plan curvature. Because concave terrain forms are associated with localized flow convergence, the negative plan-curvature values were transformed into a positive concavity layer for integration into the UGII framework.

Road-network data were obtained from OpenStreetMap through the QuickOSM plugin. The extracted line features were used to calculate road density within a 500 m search radius, generating a continuous raster surface representing neighborhood-scale infrastructure concentration and anthropogenic surface pressure.

Prior to spatial analysis, all datasets were projected to WGS 84/UTM Zone 34N (EPSG:32634), clipped to the study-area extent, resampled where necessary to a common 30 m raster grid, and spatially aligned to ensure pixel-to-pixel correspondence during subsequent indicator standardization and spatial integration.

The resulting harmonized geospatial database constituted the common analytical basis for all subsequent indicator derivation and UGII construction.

3.2. Derivation of Geoenvironmental Indicators

The proposed framework incorporates hydrological, morphometric, thermal, vegetation, and anthropogenic indicators derived from EO data, Digital Elevation Model (DEM) analysis, and urban infrastructure datasets. The selected indicators were chosen to represent complementary environmental processes associated with surface moisture accumulation, runoff concentration, terrain response, thermal stress, vegetation buffering capacity, urban sealing, and infrastructure intensity.

The indicator derivation procedure transformed heterogeneous geospatial information into spatially continuous raster layers suitable for subsequent standardization and integration during UGII construction. Hydrological and terrain-related indicators were derived from a 30 m spatial-resolution DEM provided by the Hellenic Cadastre, while vegetation and thermal indicators were extracted from Landsat 9 imagery. Anthropogenic influence was represented by road-network density derived from OpenStreetMap data. Overall, these indicators characterize the principal hydrological, geomorphological, thermal, ecological, and anthropogenic dimensions that govern the geoenvironmental dynamics of the study area, providing the analytical basis for subsequent standardization and integration within the proposed Urban Geoenvironmental Impact Index (UGII).

3.2.1. Hydrological Indicators

Hydrological conditions represent a fundamental component of urban environmental susceptibility as they control runoff generation, moisture accumulation, and the spatial

concentration of surface water. Two complementary indicators were derived to represent these processes: Flow Accumulation and the Topographic Wetness Index (TWI).

Flow Accumulation was calculated from the hydrologically conditioned DEM and represents the number of upstream cells contributing runoff to each location. Higher values identify preferential flow pathways and areas where runoff is likely to concentrate during precipitation events. Because the distribution of flow accumulation values is typically highly skewed, a logarithmic transformation was applied prior to subsequent analysis.

The Topographic Wetness Index (TWI) was calculated as:

$$TWI = ln(\frac{A_s}{tan\beta}) \quad (1)$$

where A_s represents the specific catchment area and β represents the local slope angle (Equation (1)). TWI expresses the tendency of terrain to accumulate and retain moisture. Higher values indicate sectors with increased potential for water concentration and prolonged surface wetness, while lower values characterize well-drained locations.

Together, Flow Accumulation and TWI characterize complementary components of the urban hydrological system by representing runoff-routing processes and terrain-controlled moisture accumulation, respectively.

3.2.2. Terrain Indicators

Terrain morphology strongly influences the movement, concentration, and redistribution of surface water across the urban landscape. To characterize these controls, slope and plan curvature were derived from the DEM.

Slope was calculated in degrees and expresses the local terrain gradient. Steeper slopes are associated with increased runoff velocity and enhanced downslope water transfer, whereas lower-gradient areas favour water retention and localized accumulation.

Plan curvature was used to identify terrain configurations that influence the lateral convergence or divergence of surface flow. Negative curvature values represent concave terrain forms that favour flow concentration, whereas positive values indicate divergent surfaces. Because the study focuses on susceptibility associated with hydrological convergence, negative curvature values were transformed into a positive concavity layer suitable for integration into the UGII.

Together, these terrain indicators describe the geomorphological controls regulating runoff organization and hydrological response across the study area.

3.2.3. Thermal and Urban Indicators

Thermal stress, urban sealing, vegetation distribution, and infrastructure concentration represent key dimensions of the urban geoenvironment. To capture these characteristics, Land Surface Temperature (LST), the Normalized Difference Built-up Index (NDBI), the Normalized Difference Vegetation Index (NDVI), and Road Density were incorporated into the UGII model.

Land Surface Temperature (LST) was derived from the Landsat 9 thermal infrared product and used as a direct indicator of surface thermal conditions. Elevated LST values are associated with urban heat accumulation, reduced evaporative cooling, and intensified thermal stress.

The Normalized Difference Built-up Index (NDBI) was derived from Landsat 9 imagery using its standard formulation and was employed to represent built-up intensity and urban sealing. Higher NDBI values indicate increased concentrations of impervious surfaces and anthropogenic land-cover modification.

The Normalized Difference Vegetation Index (NDVI) was also derived from Landsat 9 imagery using its standard formulation. NDVI was incorporated as an inverse geoenvironmental indicator because vegetation contributes to thermal regulation, infiltration potential, moisture retention, and environmental buffering. Consequently, areas with higher vegetation density are generally associated with lower environmental susceptibility. NDVI and NDBI were calculated using standard formulations widely adopted in remote sensing studies.

Road Density was derived from OpenStreetMap road-network data using a moving-window density analysis with a 500 m search radius. The resulting raster surface represents neighbourhood-scale infrastructure concentration and serves as a proxy for anthropogenic influence, urban structural intensity, and landscape fragmentation.

NDBI and road density were retained as independent criteria. A pixel-wise correlation across the study area (Pearson $r = -0.37$, Spearman $\rho = -0.42$, $N \approx 4.0 \times 10^5$) confirms they are weakly and negatively associated, capturing complementary and partly opposing dimensions of urbanization—spectral surface imperviousness versus infrastructural network pressure—rather than redundant information.

Precipitation intensity was represented by the annualized 99th-percentile daily precipitation contribution (R99p), computed from the wet-day ($\geq$1 mm) fraction of the 1995–2024 daily ERA5-Land record [31] following standard practice for precipitation extremes indices [32], then annualized and interpolated from the native 0.1° grid to the 30 m analysis resolution using a thin-plate-spline radial basis function, selected to avoid the discontinuous interpolation-boundary artefacts produced by standard linear interpolation given the sparse (11-cell) valid-land configuration within the study domain. This interpolation does not increase the effective spatial information content of the native ERA5-Land resolution; fine-scale (sub-9 km) spatial variability in the resulting R99p layer reflects the interpolation surface rather than genuine sub-grid climatic variability.

Overall, these indicators describe the thermal, ecological, and anthropogenic dimensions of the metropolitan environment, complementing the hydrological and geomorphological components of the proposed approach (Figure 2).

The derived indicators represent heterogeneous geospatial variables expressed in different units and value ranges. Consequently, a standardization procedure was required before their integration within the UGII framework. Both linear normalization and fuzzy membership transformations were therefore applied to generate comparable standardized surfaces suitable for multi-criteria analysis.

3.3. Indicator Standardization

Before spatial integration, all raster indicators were aligned to a common 30 m grid and transformed into dimensionless standardized surfaces ranging from 0 to 1. Two alternative standardization approaches were applied: linear min–max normalization for the conventional AHP-based model and non-linear fuzzy membership transformation for the fuzzy-AHP formulation.

Standardization converts heterogeneous geospatial variables into comparable dimensionless values while preserving their relative environmental response. In this study, both conventional linear normalization and fuzzy membership transformation were implemented to evaluate the influence of alternative standardization strategies on the resulting UGII.

3.3.1. Linear Normalization

For the conventional UGII formulation, each indicator was standardized using min–max normalization (Equation (2)):

$$N_i = \frac{X_i - X_{\text{i,min}}}{X_{\text{i,max}} - X_{\text{i,min}}} \quad (2)$$

where (X) is the original raster value, (X_{min}) and (X_{max}) are the minimum and maximum values observed within the study area, and (N_i) is the normalized standardized value ranging from 0 to 1. Minor differences between numerical ranges obtained from the full raster outputs and those calculated within the final 104.3 km^2 study-area mask result from spatial clipping to the study-area boundary. Unless otherwise specified, all area-based statistics, normalized ranges, and comparative results reported in this study refer exclusively to the final study-area extent.

For indicators expected to contribute positively to urban environmental susceptibility, higher raster values were assigned higher normalized scores. This approach was applied to flow accumulation, TWI, slope, concave curvature, LST, NDBI, and road density.

NDVI was treated inversely because higher vegetation presence is associated with stronger environmental buffering, reduced thermal stress, and increased infiltration potential. The normalized NDVI layer was therefore inverted as follows (Equation (3)):

$$NDVI_{\text{risk}} = 1 - NDVI_{\text{norm}} \quad (3)$$

The observed value ranges used for linear normalization are presented in Table 2.

Table 2. Observed indicator ranges used for linear normalization.

Indicator	Minimum	Maximum	Direction of Susceptibility
Log-transformed flow accumulation	0.301030	4.539096	Increasing
TWI	1.125519	20.083706	Increasing
R99p (mm $year^{-1}$)	26.958	31.692	Increasing
Slope	0	52.089304	Increasing
Concave plan curvature	0	0.266155	Increasing
LST (°C)	16.713440	49.177795	Increasing
NDBI	−0.392606	0.230815	Increasing
NDVI	−0.153199	0.534353	Decreasing
Road Density	0	0.070614	Increasing

The resulting normalized layers were subsequently integrated with the AHP-derived weights to construct the conventional UGII surface.

3.3.2. Fuzzy Membership Functions

Linear normalization assumes that the contribution of an indicator to environmental susceptibility increases proportionally across the full range of each indicator. This assumption is not always appropriate for urban environmental systems, where low values may exert limited influence, intermediate values may represent transition zones, and high values may produce rapidly increasing pressure before reaching saturation.

The selection of sigmoidal membership functions was based on the expected environmental behaviour of each indicator and its relationship with cumulative urban susceptibility. Sigmoidal functions were considered appropriate because they allow gradual transitions, emphasize environmentally meaningful thresholds, and accommodate saturation effects frequently observed in urban environmental systems.

To account for these non-linear relationships, each indicator was transformed into a fuzzy membership surface ranging from 0 to 1. Increasing sigmoidal membership functions were applied to indicators positively associated with susceptibility (Equation (4)):

$$\mu(x) = \frac{1}{1 + e^{-k(x-c)}} \tag{4}$$

where (μ(x)) is the fuzzy membership value, (x) is the original raster value, (k) controls the steepness of the transition, and (c) represents the midpoint at which membership equals 0.5.

For NDVI, a decreasing sigmoidal function was applied (Equation (5)):

$$\mu_{\mathrm{NDVI}}(x) = 1 - \frac{1}{1 + e^{-k(x-c)}} \tag{5}$$

This transformation assigns higher standardized values to areas with limited vegetation cover and lower values to areas with stronger vegetation presence.

The fuzzy-function parameters were selected according to the observed indicator distributions, their physical interpretation, and their environmental significance within the study area. The objective was to reduce the influence of weak signals, preserve meaningful transition zones, and emphasize sectors where environmental pressure becomes increasingly pronounced. The resulting membership functions and their parameters are summarized in Table 3.

Table 3. Fuzzy membership functions applied to the UGII indicators. Midpoint (c) and steepness (k) values for R99p were derived statistically from the sample distribution; values for the remaining indicators were calibrated through expert interpretation of each variable's observed range (see Section 3.3).

Indicator	Membership Function	Midpoint (c)	Steepness (k)	Susceptibility Role
Flow accumulation	Increasing sigmoid	2.7	4	Emphasizes runoff concentration pathways
TWI	Increasing sigmoid	10	0.6	Identifies zones of increasing moisture-accumulation potential
R99p (precipitation intensity)	Increasing sigmoid	28.805	1.100	Represents climatic extreme-precipitation forcing
Slope	Increasing sigmoid	18	0.18	Highlights terrain sectors with stronger runoff acceleration
Concave plan curvature	Increasing sigmoid	0.08	35	Emphasizes localized flow-convergence zones
LST (°C)	Increasing sigmoid	34	0.35	Identifies thermal-pressure hotspots
NDBI	Increasing sigmoid	0.02	10	Represents increasing built-up and sealing intensity
NDVI	Decreasing sigmoid	0.18	10	Assigns higher susceptibility to areas with limited vegetation buffering
Road Density	Increasing sigmoid	0.035	90	Represents neighbourhood-scale infrastructure pressure

Prior to fuzzy transformation, invalid and NoData pixels in the LST raster were removed to prevent propagation of undefined values during raster integration. The detailed parameterization of all fuzzy membership functions, including the selected midpoint (c) and steepness (k) values, is provided in Supplementary Table S1. The resulting standardized fuzzy layers were combined with the AHP-derived weights to construct the fuzzy-AHP formulation of the UGII.

3.4. AHP Weight Determination

The relative importance of the nine geoenvironmental indicators incorporated into the Urban Geoenvironmental Impact Index (UGII) was determined using the Analytic Hierarchy Process (AHP). AHP enables the systematic comparison of heterogeneous environmental and anthropogenic variables by assigning relative priorities through a pairwise comparison matrix. AHP was selected because it delivers a transparent and reproducible mechanism for incorporating expert knowledge into multi-criteria spatial analysis while providing an objective assessment of judgement consistency through the Consistency Ratio (CR).

Each indicator was compared against every other indicator using the Saaty scale, where a value of 1 indicates equal importance and values from 3 to 9 represent progressively stronger preference for one indicator over another. Reciprocal values were assigned when the indicator listed in the column was considered more important than the corresponding indicator listed in the row.

The pairwise comparisons were established according to the expected contribution of each indicator to cumulative urban environmental susceptibility. The weighting scheme was intentionally designed to reflect the conceptual importance of each environmental process within the cumulative geoenvironmental susceptibility framework rather than to reproduce historical hazard frequencies or calibrate the model against a specific hazard inventory. Consequently, the assigned priorities express expert knowledge regarding the relative contribution of each indicator to cumulative environmental susceptibility. Greater importance was assigned to hydrological indicators, particularly the Topographic Wetness Index (TWI) and flow accumulation, because they directly characterize moisture accumulation potential and preferential runoff pathways. Land Surface Temperature (LST) and the Normalized Difference Built-up Index (NDBI) were also assigned relatively high priorities due to their association with thermal pressure, urban sealing, and anthropogenic surface transformation. Road density, slope, NDVI, and concave curvature were incorporated as complementary indicators representing infrastructure concentration, terrain response, vegetation buffering, and localized flow convergence.

The pairwise comparison matrix is presented in Table 4.

Table 4. AHP pairwise comparison matrix for the UGII indicators.

	TWI	Flow Accumulation	Rainfall	Slope	Concave Curvature	LST	NDBI	NDVI	Road Density
TWI	1	3	1	5	7	2	2	4	5
Flow Accumulation	1/3	1	1/2	3	5	2	3	5	4
Rainfall	1	2	1	5	6	2	3	3	4
Slope	1/5	1/3	1/5	1	3	1/3	1/3	3	1/2
Concave Curvature	1/7	1/5	1/6	1/3	1	1/5	1/5	1/2	1/5
LST	1/2	1/2	1/2	3	5	1	2	4	3
NDBI	1/2	1/3	1/3	3	5	1/2	1	4	2
NDVI	1/4	1/5	1/3	1/3	2	1/4	1/4	1	1/3
Road Density	1/5	1/4	1/4	2	5	1/3	1/2	3	1

To confirm that the precipitation criterion does not duplicate information already captured by the remaining eight indicators, pixel-wise Pearson and Spearman correlations were computed between R99p and each of the other criteria across the study area ($N \approx 115{,}430$). All coefficients remained below the 0.6 threshold adopted in this study as a screening criterion for potential redundancy in multi-criteria frameworks ($|r| \leq 0.508$). The strongest association was observed with LST ($r = -0.508$, $\rho = -0.524$), reflecting the coincidence of higher extreme-precipitation intensity in the less urbanized, terrain-proximal northern sector with comparatively lower surface temperatures; this moderate negative association is physically coherent rather than indicative of duplicated information and falls short of the redundancy threshold. All remaining pairwise correlations were weak

($|r| \leq 0.26$), confirming that the precipitation criterion contributes complementary rather than redundant information to the UGII framework.

The resulting Consistency Ratio (CR = 0.0537) is well below the commonly accepted threshold of 0.10, indicating satisfactory consistency of the expert judgements and supporting the reliability of the derived weighting scheme. Pairwise comparisons were elicited from a single domain expert (the author); no group consensus process was applied, and this is acknowledged as a methodological limitation (Section 5.4). The robustness of the resulting susceptibility ranking to this single-expert weighting scheme is examined through the sensitivity analysis presented in Section 5.2. The final weights are presented in Table 5. The satisfactory consistency ratio indicates that the weighting scheme is internally coherent and suitable for supporting the subsequent GIS-based multi-criteria integration.

Table 5. Final AHP weights assigned to the UGII indicators.

Indicator	AHP Weight	Relative Priority	Environmental Dimension
TWI	0.228	Highest	Moisture accumulation potential
Rainfall (R99p)	0.210	Very High	Extreme precipitation forcing
Flow Accumulation	0.160	High	Runoff concentration pathways
LST	0.126	High	Thermal stress
NDBI	0.099	High	Urban sealing and built-up intensity
Road Density	0.066	Moderate	Infrastructure pressure
Slope	0.051	Moderate	Terrain-controlled runoff response
NDVI	0.037	Low	Vegetation buffering capacity
Concave Plan Curvature	0.023	Low	Localized flow convergence
Total	1.000		

To ensure a consistent comparison between the conventional and fuzzy formulations, the AHP weights were applied identically in both models. Consequently, any differences observed in the resulting UGII surfaces can be attributed exclusively to the alternative standardization strategies rather than to changes in indicator weighting.

3.5. Construction of the Urban Geoenvironmental Impact Index (UGII)

The Urban Geoenvironmental Impact Index (UGII) was generated through the weighted spatial integration of the standardized geoenvironmental indicators. Two complementary formulations were developed: a conventional AHP-based model using linearly normalized indicators and a fuzzy-AHP model using non-linear fuzzy membership surfaces. The same AHP-derived weights were applied in both cases to isolate the effect of indicator standardization on the final spatial pattern [33,34].

3.5.1. Classical AHP-UGII

The conventional UGII formulation was calculated through a weighted linear combination of the normalized indicator rasters (Equations (6) and (7)):

$$UGII_{\mathrm{AHP}} = \sum_{i=1}^{n} w_i N_i \tag{6}$$

where

- $UGII_{AHP}$ is the conventional Urban Geoenvironmental Impact Index;
- w_i is the AHP-derived weight assigned to indicator (i);
- N_i is the linearly standardized raster value of indicator (i);
- n is the total number of indicators included in the model.

For the present study, the formulation was expressed as:

$$UGII_{\text{AHP}} = 0.228\ (TWI_{\text{norm}})\ +\ 0.160\ (FA_{\text{norm}}) + 0.210\ (R99p_{\text{norm}}) +\ 0.051\ (Slope_{\text{norm}}) + 0.023\ (Curvature_{\text{norm}})\ +\ 0.126\ (LST_{\text{norm}})\ +\ 0.099\ (NDBI_{\text{norm}}) + 0.037\ (NDVI_{\text{risk}})\ +\ 0.066\ (RD_{\text{norm}}) \quad (7)$$

where FA represents log-transformed flow accumulation, R99p represents the annualized 99th-percentile daily precipitation contribution, and RD represents road density.

This formulation produces a continuous susceptibility surface in which higher values indicate stronger cumulative urban environmental susceptibility.

3.5.2. Fuzzy-AHP UGII Formulation

The fuzzy-AHP formulation was developed using the same AHP weights but replacing the linearly normalized rasters with fuzzy membership surfaces (Equation (8)):

$$UGII_{\text{Fuzzy}} = \sum_{i=1}^{n} (w_i \times F_i) \quad (8)$$

where

- $UGII_{\text{Fuzzy}}$ is the fuzzy Urban Geoenvironmental Impact Index;
- w_i is the AHP-derived weight assigned to indicator (i);
- F_i is the fuzzy membership value of indicator (i), ranging from 0 to 1;
- n is the total number of indicators included in the model.

The final fuzzy formulation was expressed as (Equation (9)):

$$UGII_{\text{Fuzzy}} = 0.228\ (TWI_{\text{fuzzy}})\ +\ 0.160\ (FA_{\text{fuzzy}})\ +\ 0.210\ (R99p_{\text{fuzzy}}) +\ 0.051\ (Slope_{\text{fuzzy}}) + 0.023\ (Curvature_{\text{fuzzy}})\ +\ 0.126\ (LST_{\text{fuzzy}})\ +\ 0.099\ (NDBI_{\text{fuzzy}}) + 0.037\ (NDVI_{\text{fuzzy}})\ +\ 0.066\ (RD_{\text{fuzzy}}) \quad (9)$$

The fuzzy-AHP model preserves the relative importance structure defined through AHP while representing the non-linear environmental response of each indicator. This approach reduces the influence of weak signals, emphasizes meaningful transition zones, and produces a more continuous and coherent susceptibility surface. The implementation of both the conventional and fuzzy-based formulations enables a direct comparison between linear weighted-overlay modelling and uncertainty-aware geoenvironmental assessment.

Both UGII surfaces were classified into five relative susceptibility classes using the Natural Breaks (Jenks) classification method, which identifies class boundaries by maximizing within-class similarity and between-class differences [35]:

- Very Low;
- Low;
- Moderate;
- High;
- Very High.

The classified surfaces were used for comparative evaluation and for the subsequent assessment of built assets and real-estate exposure.

3.6. Built-Asset Exposure Assessment

3.6.1. Built-Asset Layer

The built-asset exposure component of the study was based on the spatial distribution of built assets within the study area. Built assets constitute the physical concentration of residential, commercial, industrial, and infrastructure-related structures that may be exposed to environmental susceptibility.

A built-asset layer was developed using building-footprint information obtained from OpenStreetMap. Individual building polygons were converted into a continuous density surface through kernel-density estimation using a 300 m search radius. The resulting raster expresses the relative concentration of built assets across the southern sector of the Athens Metropolitan Area and serves as a proxy for the spatial distribution of urban development intensity.

Higher density values indicate areas presenting greater concentrations of buildings and infrastructure, whereas lower values correspond to open spaces, recreational zones, coastal sectors, and areas with limited urban development. This built-asset exposure assessment acts as a spatial proxy for real-estate exposure.

3.6.2. Exposure Model and Classification

Built-asset exposure was defined as the spatial coincidence between cumulative urban environmental susceptibility and the concentration of built assets. The underlying assumption is that environmental susceptibility acquires greater practical significance where environmental pressures overlap with dense urban development and substantial concentrations of physical assets.

To represent this interaction, the fuzzy-AHP UGII surface was combined with the normalized building-density layer through raster multiplication (Equation (10)). For consistency, the term REE is retained to denote the built-asset exposure surface, which is used here as a spatial proxy for real-estate exposure:

$$REE = UGII_{\text{Fuzzy}} \times BAD \tag{10}$$

where

- $UGII_{Fuzzy}$ is the fuzzy-AHP Urban Geoenvironmental Impact Index;
- BAD is the normalized Built-Asset Density layer.

The resulting raster highlights sectors where elevated environmental susceptibility coincides with high building concentrations. Higher values indicate areas characterized by both increased environmental pressure and substantial urban development intensity. The final exposure surface was classified into five relative exposure classes using the Natural Breaks (Jenks) classification method: Very Low, Low, Moderate, High, and Very High. These classes were used to identify priority sectors where susceptibility may have greater implications for urban planning, redevelopment planning, and built-asset management.

3.7. Metrics for Comparing the Conventional and Fuzzy UGII Models

The conventional AHP-based UGII and the fuzzy-AHP UGII surfaces were quantitatively compared in order to evaluate the effect of fuzzy standardization on the statistical and spatial characteristics of the resulting susceptibility maps. The comparison was performed using descriptive statistical measures and pixel-wise correspondence metrics calculated from the complete raster datasets.

For each UGII surface, the minimum value, maximum value, mean, standard deviation, coefficient of variation (CV), and dynamic range were calculated. The standard deviation and coefficient of variation were used to quantify the degree of spatial differentiation

represented by each model, whereas the dynamic range was used to evaluate the extent to which each formulation exploited the available susceptibility scale.

To assess the spatial consistency between the two approaches, Pearson's correlation coefficient and Spearman's rank correlation coefficient were calculated using all raster cells. These measures quantify the similarity of the spatial patterns independently of the visual comparison of the maps.

This quantitative comparison complements the visual assessment of the susceptibility maps and provides an objective evaluation of whether fuzzy standardization modifies the spatial organization of susceptibility or primarily enhances the representation of gradual environmental transitions.

4. Results

4.1. EO-Derived Indicators

The EO-derived, morphometric/terrain-hydrological, climatic, and infrastructure-related indicators reveal pronounced spatial variability in the geoenvironmental conditions of the study area across the southern sector of the Athens Metropolitan Area (Figures 3–11). The observed patterns reflect the combined influence of terrain morphology, hydrological organization, climatic forcing, urban development intensity, vegetation distribution, and thermal conditions, highlighting the heterogeneous environmental character of the study area.

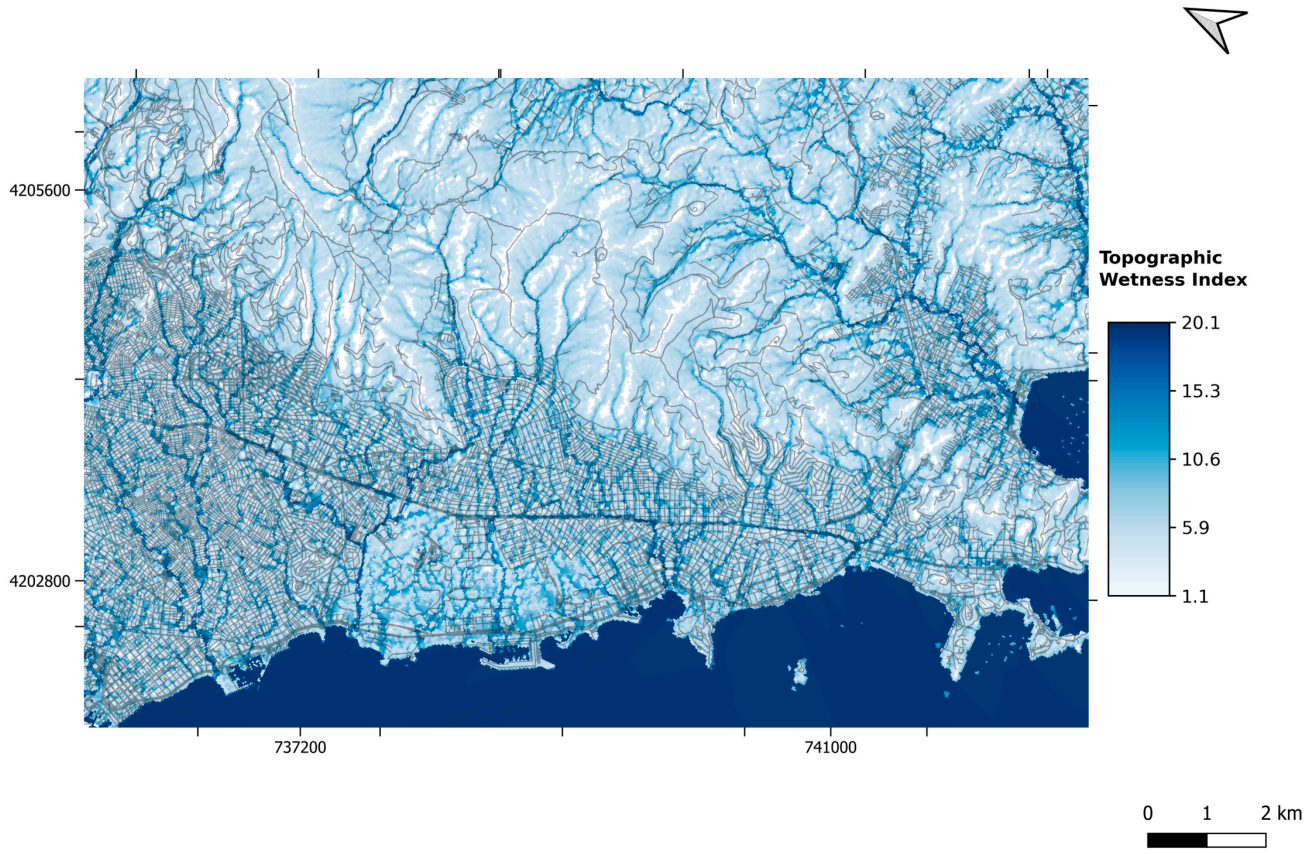


Figure 3. Spatial distribution of the Topographic Wetness Index (TWI) derived from the 30 m Digital Elevation Model (DEM) for the southern sector of the Athens Metropolitan Area, Greece. Higher TWI values indicate terrain with greater potential for moisture accumulation and surface-water concentration under topographic control.

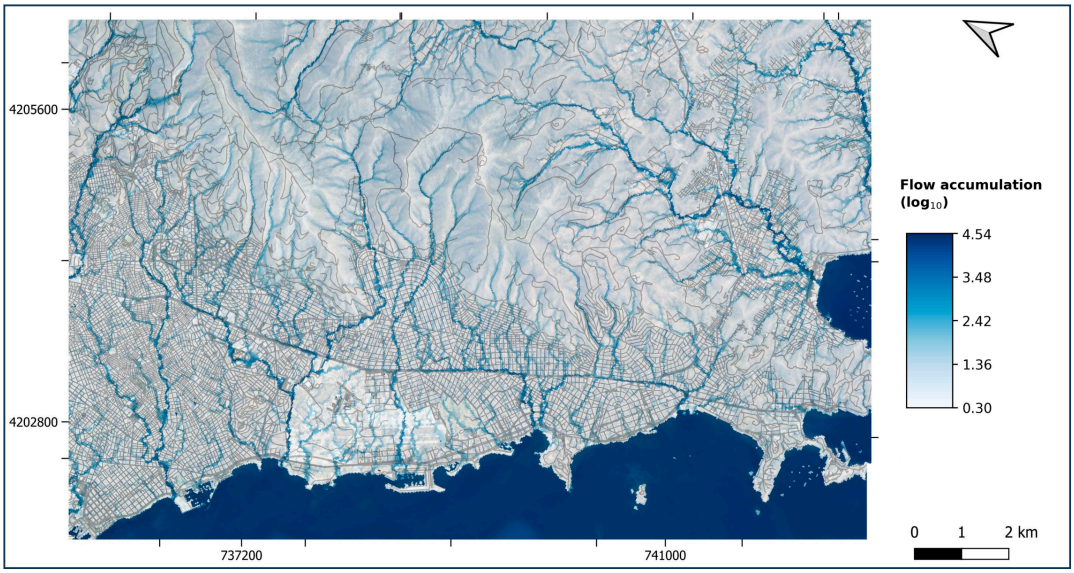


Figure 4. Spatial distribution of Flow Accumulation derived from the hydrologically conditioned 30 m Digital Elevation Model (DEM) for the southern sector of the Athens Metropolitan Area, Greece. The raster represents the logarithmically transformed upstream contributing area, highlighting preferential runoff pathways and locations where surface water is expected to concentrate during rainfall events.

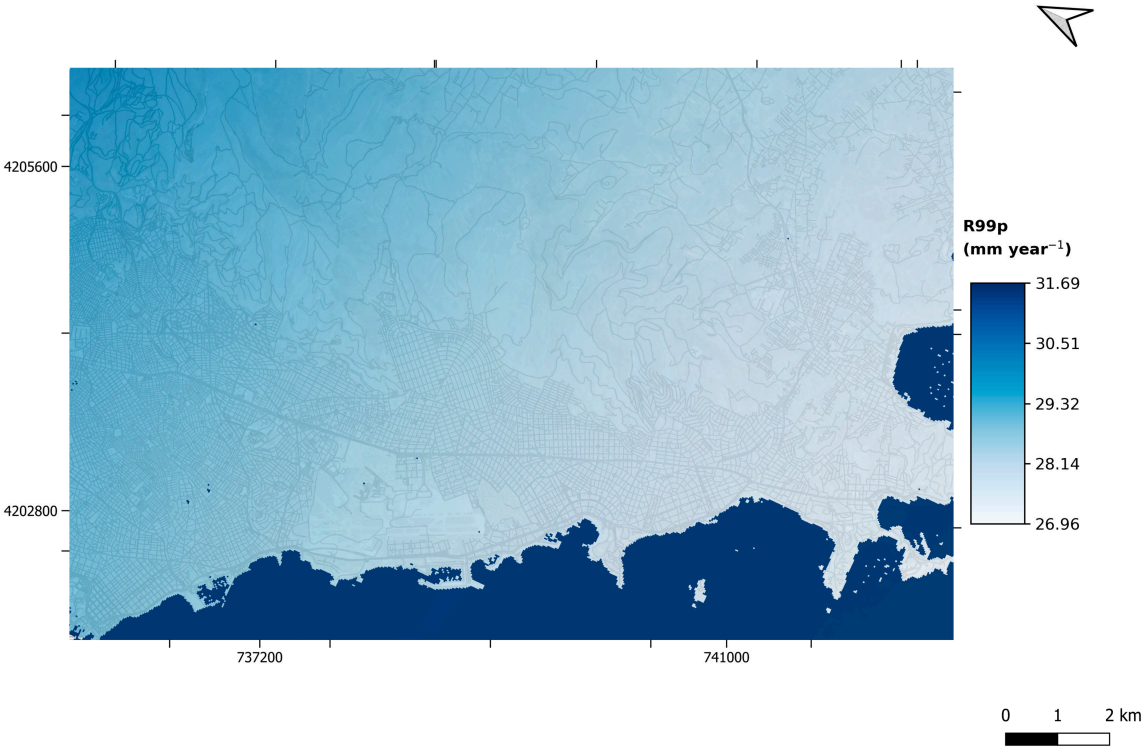


Figure 5. Spatial distribution of the annualized 99th-percentile daily precipitation contribution (R99p) derived from the ERA5-Land daily precipitation reanalysis (1995–2024) for the southern sector of the Athens Metropolitan Area, Greece. The raster represents the climatological extreme-precipitation intensity, resampled to the common 30 m analytical grid for raster integration, while retaining the effective spatial information content of the native ERA5-Land resolution, highlighting the metropolitan-scale gradient of extreme rainfall forcing across the study area.

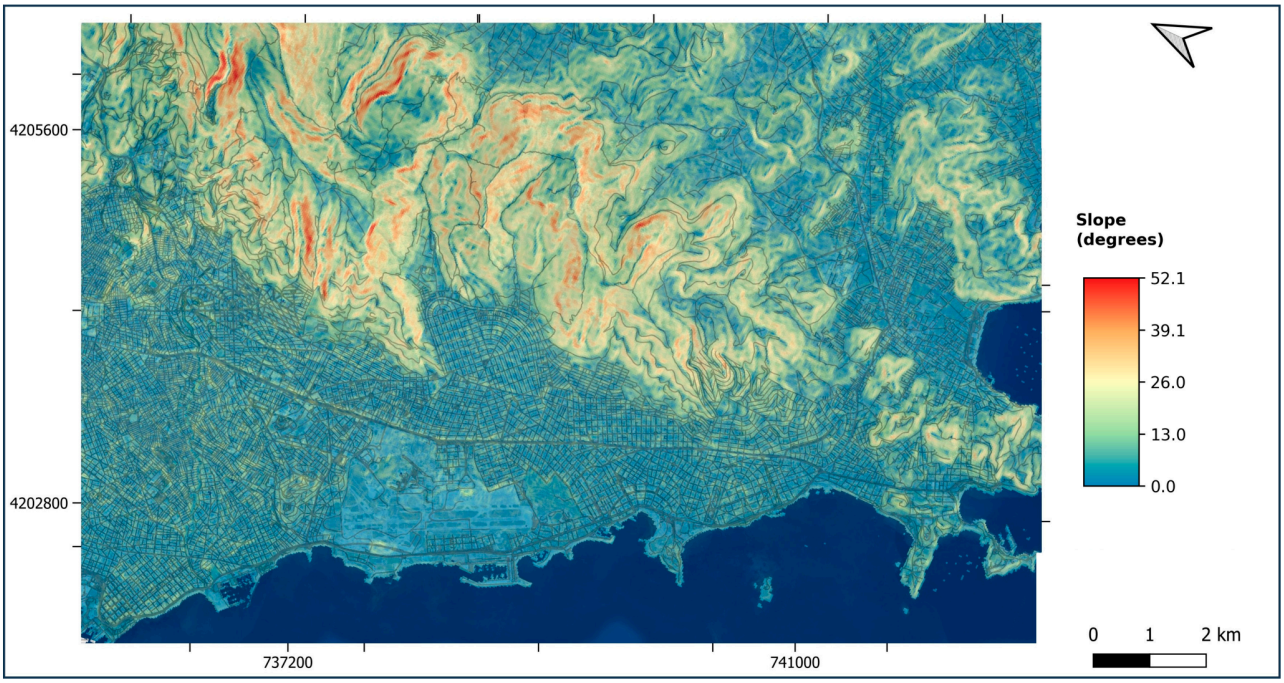


Figure 6. Spatial distribution of slope (degrees) derived from the 30 m Digital Elevation Model (DEM) for the southern sector of the Athens Metropolitan Area, Greece. Higher slope values indicate steeper terrain, which promotes faster surface runoff and influences the spatial distribution of hydrological processes.

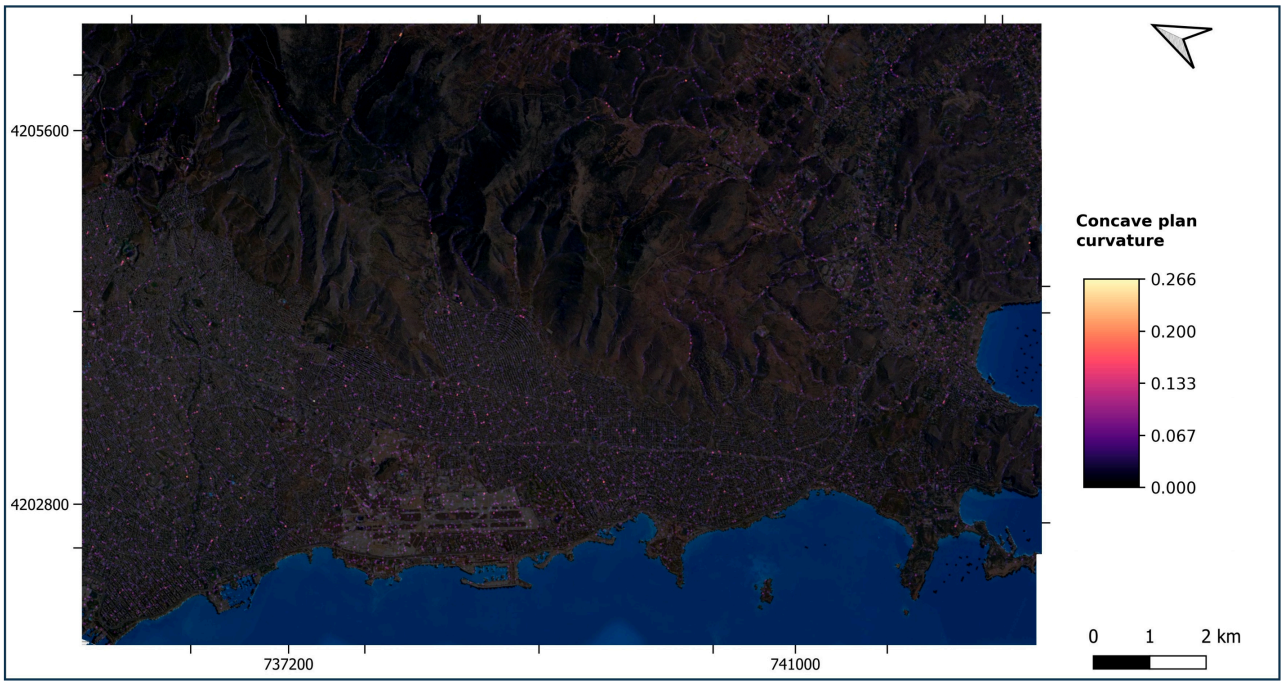


Figure 7. Spatial distribution of concave plan curvature derived from the 30 m Digital Elevation Model (DEM) for the southern sector of the Athens Metropolitan Area, Greece. Negative plan-curvature values were transformed into a positive concavity layer to emphasize terrain sectors that promote lateral flow convergence and localized surface-water accumulation.

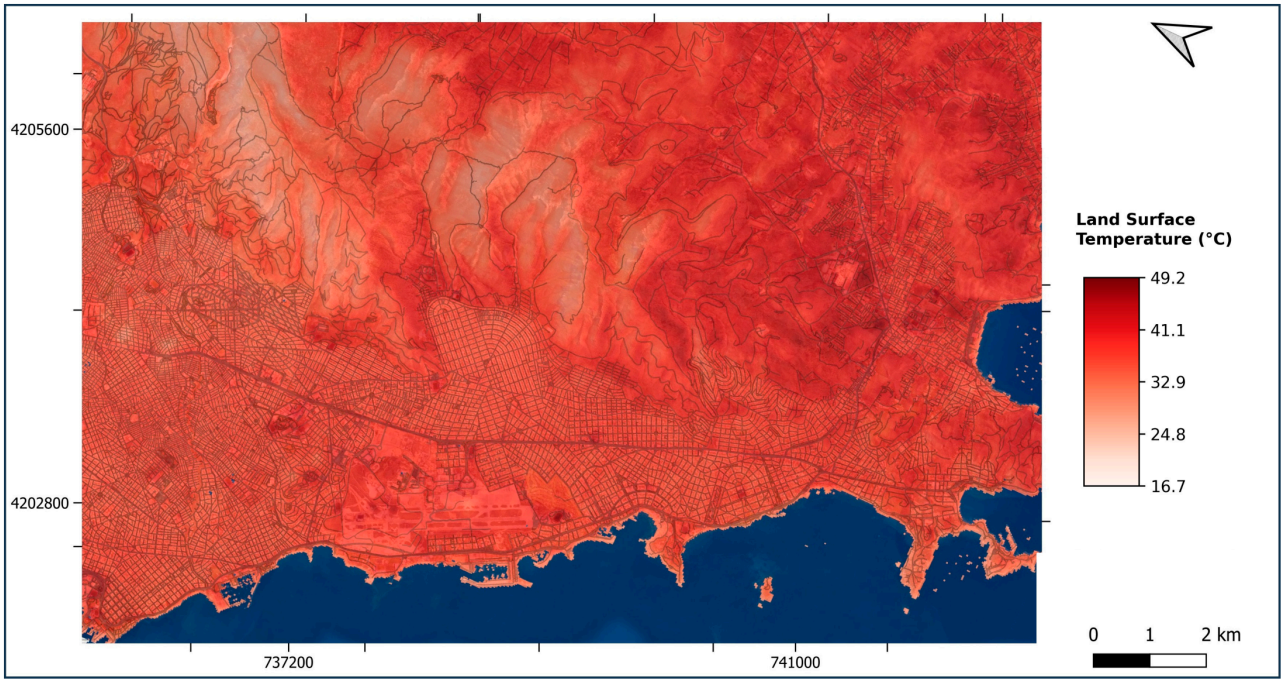


Figure 8. Spatial distribution of Land Surface Temperature (LST) (°C) derived from the Landsat 9 Collection 2 Level-2 thermal infrared product for the southern sector of the Athens Metropolitan Area, Greece. Higher temperatures identify urban thermal hotspots associated with dense built-up areas, extensive impervious surfaces, and limited vegetation cover.

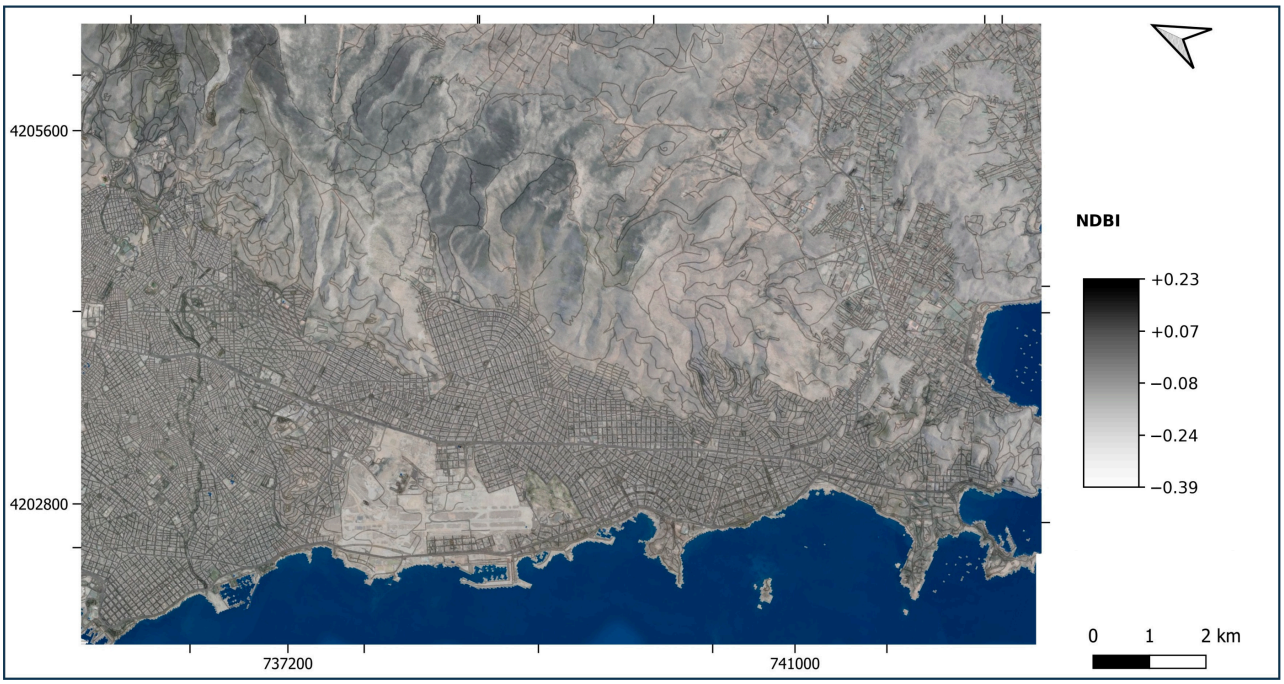


Figure 9. Spatial distribution of the Normalized Difference Built-up Index (NDBI) derived from Landsat 9 Collection 2 Level-2 surface reflectance imagery for the southern sector of the Athens Metropolitan Area, Greece. Higher NDBI values indicate greater built-up intensity, impervious surface cover, and urban sealing associated with densely developed areas.

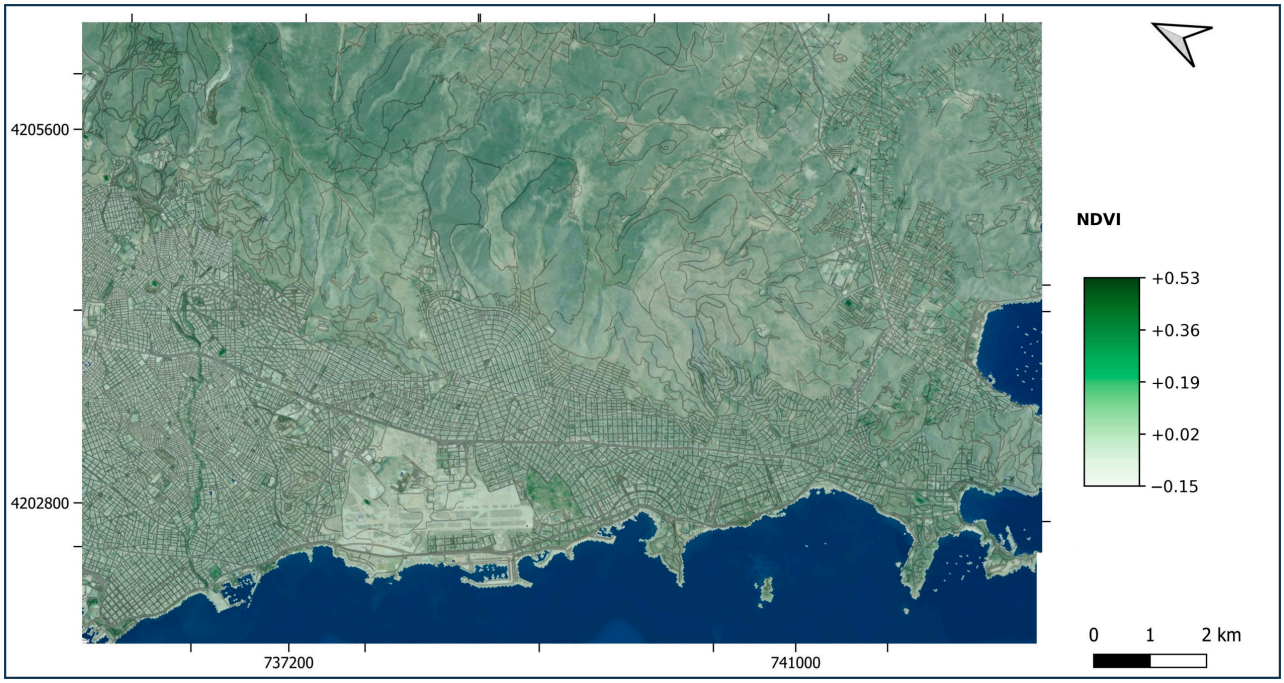


Figure 10. Spatial distribution of the Normalized Difference Vegetation Index (NDVI) derived from Landsat 9 Collection 2 Level-2 surface reflectance imagery for the southern sector of the Athens Metropolitan Area, Greece. Higher NDVI values indicate denser and healthier vegetation cover, reflecting areas with greater environmental buffering capacity, enhanced infiltration potential, and reduced surface thermal stress.

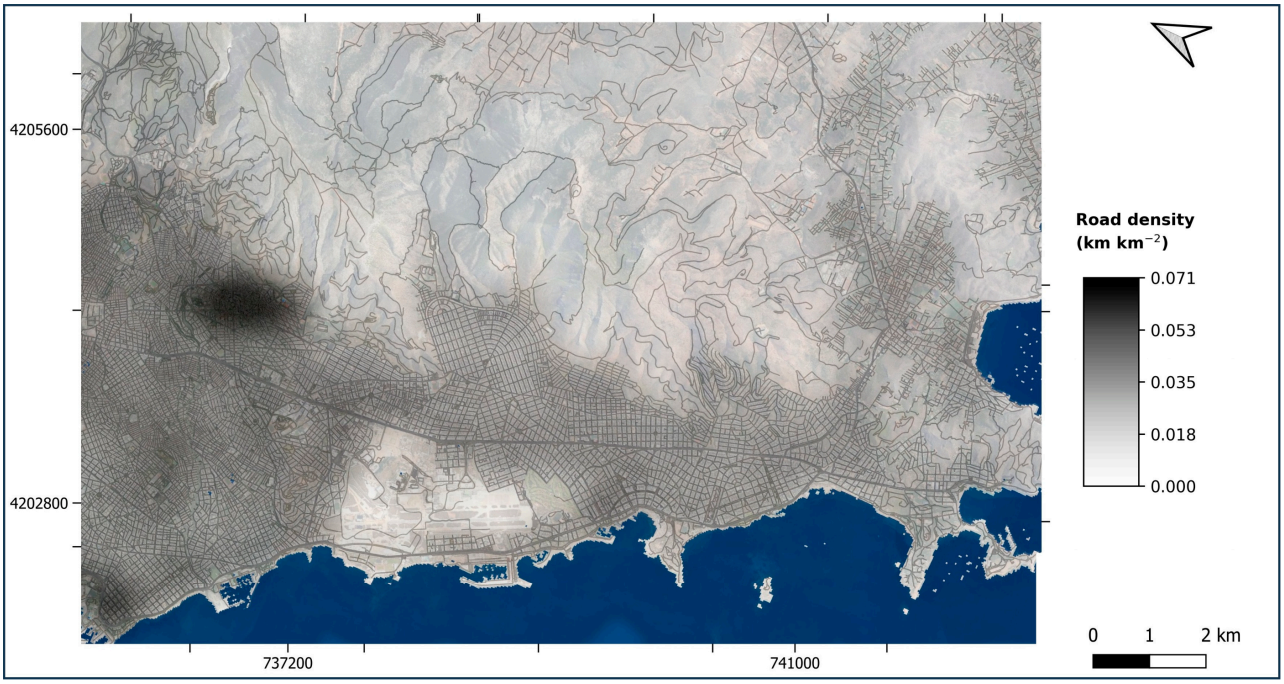


Figure 11. Spatial distribution of road density derived from the OpenStreetMap road network using a 500 m moving-window density analysis for the southern sector of the Athens Metropolitan Area, Greece. Higher road-density values indicate greater transportation infrastructure concentration, reflecting increased anthropogenic pressure, urban structural intensity, and landscape fragmentation.

The precipitation indicator (R99p) displays comparatively limited spatial variability within the study area, consistent with the metropolitan-scale extent of the domain relative

to the synoptic scale of precipitation systems (Section 3.4). A modest inland-to-coastal contrast is nevertheless discernible, with higher R99p values recorded across the northern, terrain-proximal municipalities (mean 29.8 mm year^{-1}) relative to the southern coastal sector (mean 28.8 mm year^{-1}) (Figure 5). This pattern indicates a weak but physically coherent enhancement of extreme precipitation intensity toward the inland margins of the study area.

The hydrological indicators exhibit distinct spatial concentration patterns associated with terrain-controlled runoff processes. Elevated TWI values are primarily observed within low-gradient sectors, topographically convergent areas, and drainage corridors where moisture accumulation potential is enhanced (Figure 3). Similarly, the Flow Accumulation layer identifies preferential runoff pathways and sectors with increased upstream contributing area (Figure 4). The spatial coincidence of high TWI and elevated flow accumulation values indicates areas where water concentration processes may become particularly pronounced during precipitation events.

Terrain-related indicators reveal additional controls on hydrological behaviour. Higher slope values are concentrated along the eastern and northeastern margins of the study area, where the influence of the Hymettus mountain front becomes more evident (Figure 6). In contrast, lower-gradient sectors dominate the coastal urban plain. The concave curvature layer highlights localized convergence zones where terrain morphology favours lateral concentration of surface flow (Figure 7). These morphometric characteristics influence the spatial organization of runoff pathways and contribute to the development of localized hydrological susceptibility patterns.

The thermal and land-cover indicators display strong spatial contrasts associated with urban development intensity. Land Surface Temperature (LST) identifies distinct thermal hotspots within densely urbanized sectors with extensive impervious surfaces and limited vegetation cover (Figure 8). These areas generally coincide with elevated NDBI values (Figure 9), indicating increased built-up intensity and urban sealing. Conversely, higher NDVI values are concentrated within urban green spaces, recreational areas, and sectors with greater vegetation presence (Figure 10), reflecting enhanced environmental buffering capacity and reduced thermal stress.

Road Density further illustrates the spatial distribution of anthropogenic pressure across the metropolitan landscape (Figure 11). Elevated density values occur along major transportation corridors and highly urbanized sectors, reflecting increased infrastructure concentration and landscape fragmentation. The spatial overlap between high road density, elevated NDBI values, and increased surface temperatures highlights the strong influence of urban development on environmental conditions within the study area.

Collectively, the derived indicators reveal that urban environmental susceptibility is not controlled by a single environmental factor but emerges through the interaction of hydrological accumulation, terrain morphology, climatic forcing, thermal stress, vegetation distribution, and infrastructure concentration. These spatial patterns provide the analytical basis for the subsequent construction of the conventional and fuzzy-AHP Urban Geoenvironmental Impact Index (UGII) surfaces.

4.2. Conventional AHP-Based UGII

The conventional AHP-based Urban Geoenvironmental Impact Index (UGII) was generated through the weighted linear integration of the nine standardized environmental indicators using the AHP-derived weights. The resulting susceptibility surface forms an integrated representation of environmental conditions across the southern sector of the Athens Metropolitan Area (Figure 12).

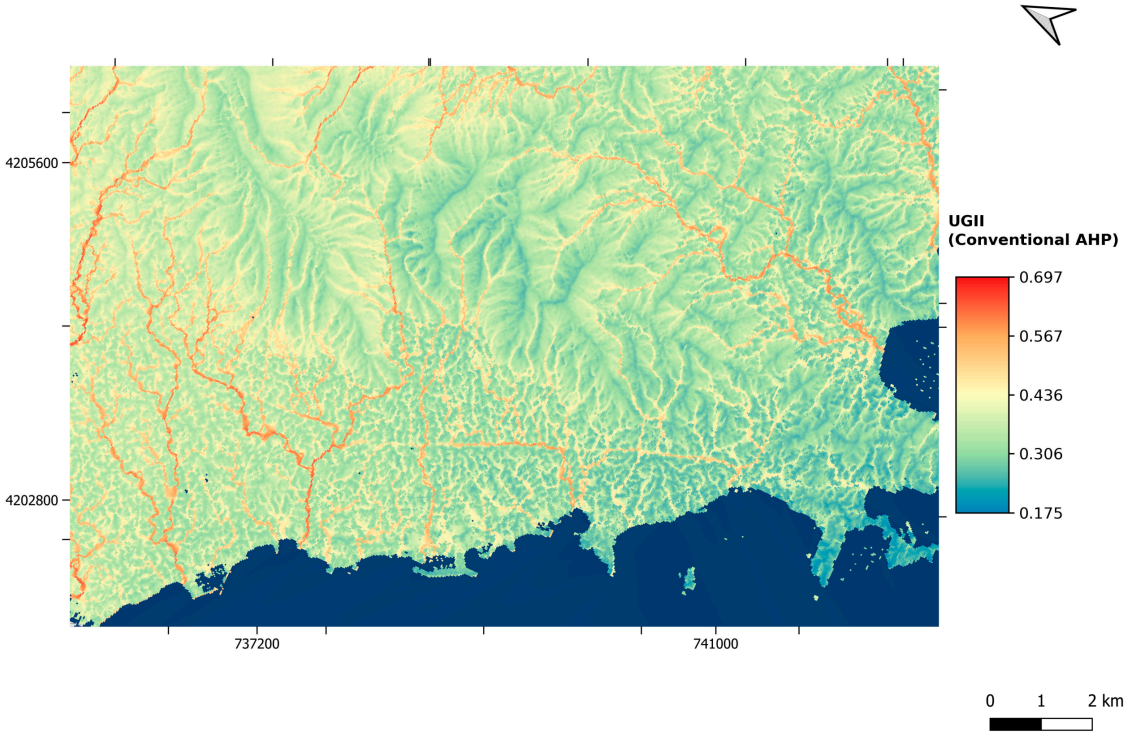


Figure 12. Spatial distribution of the conventional AHP-based Urban Geoenvironmental Impact Index (UGII) for the southern sector of the Athens Metropolitan Area, Greece. The index ranges from 0.18 to 0.65 and was classified into five relative susceptibility classes (Very Low, Low, Moderate, High, and Very High) using the Natural Breaks (Jenks) classification method. Values reported in the text refer to the seven-municipality study area (104.3 km^2); the raster legend reflects the full analysis raster extent.

The generated surface exhibits a relatively smooth spatial distribution with gradual variations in susceptibility values throughout the study area. UGII values range from approximately 0.18 to 0.64, indicating moderate spatial differentiation rather than the presence of sharply defined susceptibility hotspots. This pattern reflects the averaging effect inherent in weighted linear combination approaches, whereby individual indicator contributions are integrated into a single continuous surface.

Higher susceptibility values are generally concentrated within densely urbanized sectors and along areas where hydrological accumulation, elevated surface temperatures, increased built-up intensity, and infrastructure concentration coexist. Conversely, lower susceptibility values are primarily associated with sectors characterized by greater vegetation presence, reduced urban density, and less pronounced hydrological convergence.

A notable characteristic of the conventional UGII surface is the broad spatial continuity of susceptibility values. Transitional areas occupy a substantial proportion of the study area, producing extensive zones of moderate susceptibility between higher and lower value sectors. While this behaviour serves as a coherent regional representation of cumulative environmental conditions, it may also reduce the ability of the model to distinguish localized variations and gradual environmental transitions associated with non-linear urban processes.

Overall, the conventional AHP-based UGII establishes a baseline representation of cumulative urban environmental susceptibility and serves as the reference model for evaluating the influence of fuzzy membership transformations on the spatial characterization of susceptibility patterns.

4.3. Fuzzy-AHP UGII

The fuzzy-AHP Urban Geoenvironmental Impact Index was generated by integrating the fuzzy membership surfaces of the nine environmental indicators using the same AHP-derived weighting structure applied in the conventional model. The resulting susceptibility surface is presented in Figure 13.

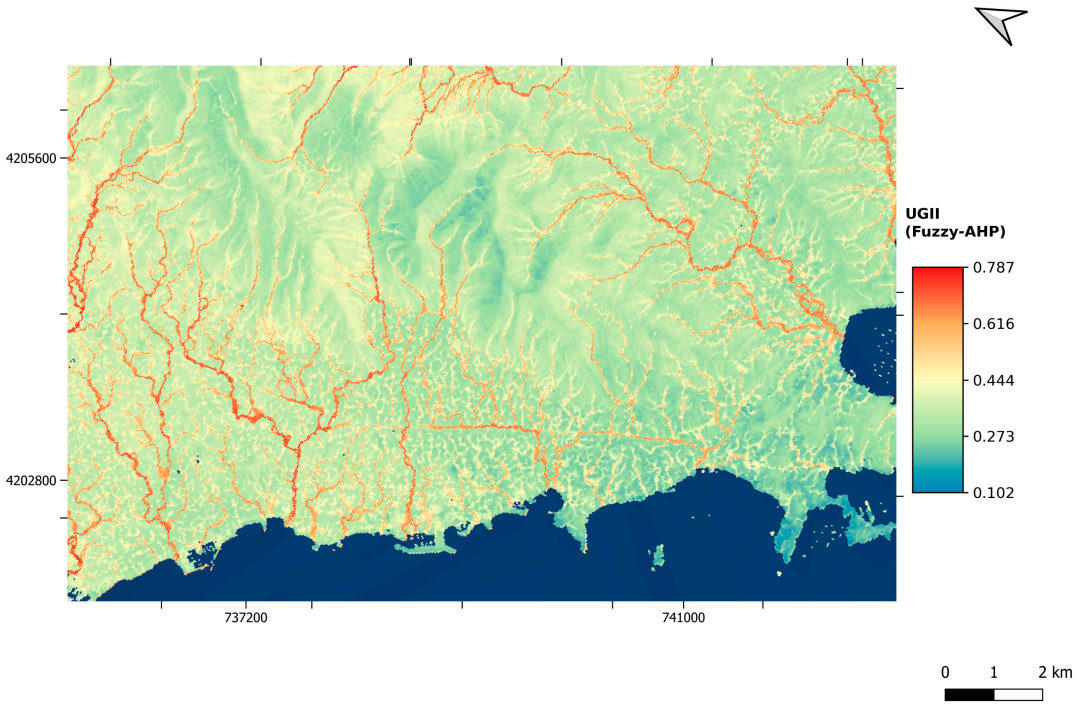


Figure 13. Spatial distribution of the fuzzy-AHP Urban Geoenvironmental Impact Index (UGII) for the southern sector of the Athens Metropolitan Area, Greece. The index ranges from 0.10 to 0.75 and was classified into five relative susceptibility classes (Very Low, Low, Moderate, High, and Very High) using the Natural Breaks (Jenks) classification method. Values reported in the text refer to the seven-municipality study area (104.3 km^2); the raster legend reflects the full analysis raster extent.

The fuzzy-AHP UGII exhibits a broader range of susceptibility values than the conventional AHP-based formulation, with values ranging from approximately 0.10 to 0.75. This wider distribution reflects the ability of fuzzy membership functions to represent gradual environmental transitions and non-linear relationships between indicator values and susceptibility conditions. As a result, the fuzzy-based model enhances the contrast between lower- and higher-susceptibility sectors while preserving the overall spatial organization of the study area.

The spatial distribution of the fuzzy-AHP surface remains generally consistent with the major susceptibility patterns identified by the conventional model. However, susceptibility gradients become more clearly expressed, particularly within sectors characterized by intermediate environmental conditions. Areas that exhibited moderate susceptibility under the conventional formulation display greater spatial differentiation, reflecting the capacity of fuzzy membership functions to capture variations that may be partially masked by linear standardization approaches.

The fuzzy formulation also enhances the representation of transition zones between low- and high-susceptibility areas. Rather than treating indicator influence as a strictly proportional response, the fuzzy approach allows susceptibility to increase or decrease according to the environmental response represented by each variable. This characteristic is particularly relevant in urban environments, where hydrological accumulation, ther-

mal stress, vegetation loss, and infrastructure concentration rarely operate through fixed thresholds or strict linear processes.

Overall, the fuzzy-AHP UGII offers a more differentiated representation of cumulative urban environmental susceptibility by incorporating uncertainty and gradual environmental transitions into the modelling process. While the principal susceptibility patterns remain spatially comparable to those identified by the conventional UGII, the fuzzy formulation produces a more differentiated susceptibility surface that is better suited to representing the complexity of urban environmental systems.

4.4. Comparative Analysis of Conventional and Fuzzy-AHP UGII

A comparative assessment was performed to evaluate the influence of fuzzy membership transformation on the spatial representation of cumulative urban environmental susceptibility. The comparison was based on the difference raster generated by subtracting the conventional AHP-based UGII from the fuzzy-AHP UGII surface (Figure 14). The resulting differences range from approximately −0.09 to 0.14, indicating that fuzzy transformation both increased and decreased susceptibility values depending on the environmental characteristics of each location. Positive values correspond to areas where the fuzzy formulation produced higher susceptibility estimates, whereas negative values represent locations where susceptibility was reduced following fuzzy transformation.

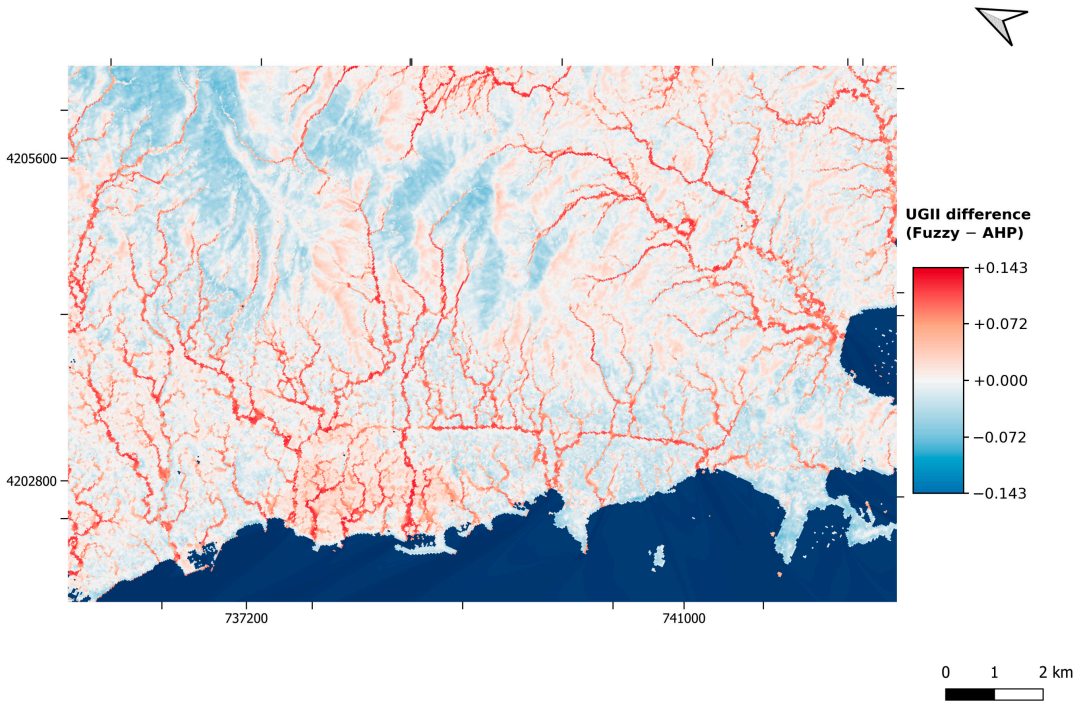


Figure 14. Spatial difference between the fuzzy-AHP and conventional AHP-based Urban Geoenvironmental Impact Index (UGII) surfaces for the southern sector of the Athens Metropolitan Area, Greece. Positive values indicate areas where the fuzzy formulation produced higher susceptibility estimates, whereas negative values indicate lower susceptibility estimates relative to the conventional model.

The difference map reveals that the overall spatial structure of susceptibility remains largely consistent between the two modelling approaches. The principal susceptibility patterns identified by the conventional UGII are preserved within the fuzzy formulation, indicating that both models recognize similar areas of environmental concern across the study area. This consistency suggests that the incorporation of fuzzy logic does not

fundamentally alter the spatial geography of susceptibility but rather modifies the way environmental influence is represented and weighted.

The observed differences are primarily concentrated within transitional sectors with intermediate indicator values and mixed environmental conditions. These areas correspond to locations where environmental behaviour cannot be adequately represented by rigid linear responses and where gradual environmental transitions are more pronounced. Under such circumstances, fuzzy membership functions allow susceptibility to vary according to the degree of environmental influence rather than through strictly proportional linear relationships.

The spatial distribution of positive and negative differences further indicates that fuzzy transformation affects mainly those areas where multiple environmental drivers interact simultaneously. Hydrological accumulation, terrain response, thermal stress, vegetation conditions, and infrastructure concentration often exhibit non-linear relationships that are difficult to capture through conventional normalization procedures. The fuzzy formulation accommodates these interactions by allowing susceptibility to increase or decrease gradually as environmental conditions evolve across space.

A notable outcome of the comparison is that the fuzzy-AHP model enhances local spatial differentiation while preserving the broader susceptibility pattern identified by the conventional approach. Areas exhibiting consistently high or consistently low susceptibility remain relatively stable, whereas intermediate zones display greater variability following fuzzy transformation. This behaviour suggests that fuzzy logic contributes primarily to the refinement of susceptibility gradients and the representation of environmental uncertainty rather than to the generation of entirely new susceptibility patterns.

Overall, the comparative analysis demonstrates that the fuzzy-AHP formulation functions as an enhancement of the conventional weighted-overlay approach. By incorporating gradual transitions and non-linear environmental responses, the fuzzy model provides a more realistic representation of cumulative urban environmental susceptibility while maintaining consistency with the principal spatial patterns identified by the conventional UGII. These findings support the use of fuzzy geoenvironmental approaches for the assessment of complex urban environmental systems where uncertainty and gradual environmental transitions play an important role in shaping spatial susceptibility patterns.

The comparison demonstrates that fuzzy standardization primarily refines the spatial representation of environmental susceptibility rather than fundamentally altering the spatial structure identified by the conventional model. This finding indicates that the incorporation of fuzzy membership functions enhances the characterization of gradual environmental transitions while preserving the overall geographical consistency of the assessment.

4.5. Quantitative Comparison of the Conventional and Fuzzy UGII Models

To complement the visual comparison presented in Section 4.4, the two UGII surfaces were quantitatively compared using descriptive statistics and pixel-wise correspondence metrics (Table 6). The quantitative comparison confirms that the fuzzy-AHP formulation substantially increases the spatial variability of the susceptibility surface while preserving the overall spatial organization of the conventional model.

The standard deviation increased from 0.068 to 0.093 (approximately 37%), indicating stronger local spatial differentiation. Similarly, the coefficient of variation increased from 0.183 to 0.240, demonstrating greater relative dispersion of susceptibility values.

The fuzzy formulation also expanded the dynamic range of the UGII from 0.522 to 0.684 (approximately 31%), indicating that fuzzy standardization more effectively exploits

the available susceptibility range and enhances the discrimination between areas exhibiting different levels of cumulative environmental susceptibility.

Table 6. Quantitative comparison between the conventional AHP-UGII and fuzzy-AHP UGII surfaces.

Metric	Conventional AHP	Fuzzy-AHP
Mean	0.372	0.387
Standard deviation	0.068	0.093
Coefficient of variation	0.183	0.240
Dynamic range	0.522	0.684
Pearson correlation	0.942 *	
Spearman correlation	0.916 *	

* Pearson and Spearman correlation coefficients quantify the agreement between the two raster surfaces.

Despite these differences, both models remain highly consistent spatially. Pearson's correlation coefficient (r = 0.942) and Spearman's rank correlation coefficient (ρ = 0.916) indicate that the fuzzy formulation preserves the principal susceptibility pattern identified by the conventional AHP model while refining local transitions and improving the representation of intermediate environmental conditions.

4.6. Urban Susceptibility Hotspots and Real-Estate Exposure

The integration of fuzzy-AHP susceptibility modelling with building-density information enables the identification of urban sectors where cumulative environmental pressures coincide with concentrated urban development. The resulting Built-Asset Density (BAD) layer and the derived Real-Estate Exposure (REE) surface provide complementary information for evaluating the spatial relationship between environmental susceptibility and urban development intensity.

The normalized Built-Asset Density (BAD) layer, which represents the spatial concentration of buildings independently of environmental susceptibility, is presented in Figure 15. This layer constitutes the exposure component of the proposed framework and forms the basis for the calculation of the Real-Estate Exposure (REE) surface.

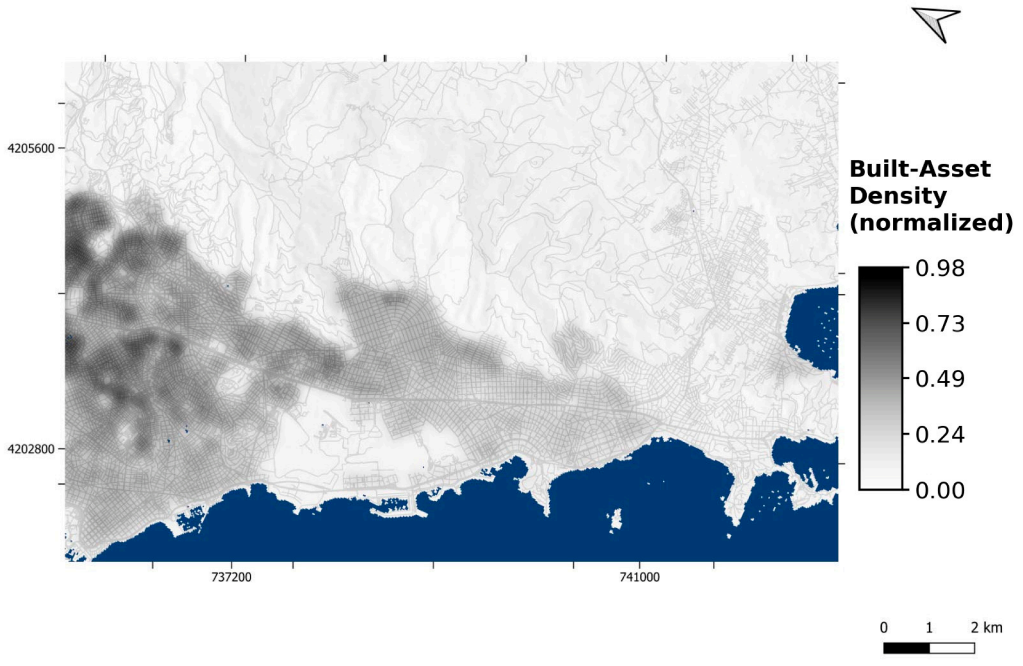


Figure 15. Spatial distribution of the normalized Built-Asset Density (BAD) layer derived from OpenStreetMap building footprints using kernel density estimation (300 m search radius). Higher values indicate increasing concentrations of buildings and urban development.

The spatial distribution of exposure exhibits a heterogeneous pattern reflecting the combined influence of hydrological conditions, terrain configuration, thermal stress, urban sealing, infrastructure concentration, and building density. High and very high exposure classes occur in sectors where elevated susceptibility values overlap with dense urban development, indicating locations where environmental pressures and urban development intensity interact most strongly.

The identified exposure hotspots are primarily concentrated within the highly urbanized coastal and metropolitan sectors of the study area. These areas exhibit dense building concentrations, extensive transportation infrastructure, elevated surface temperatures, and increased levels of urban sealing. The convergence of these environmental and anthropogenic factors results in greater cumulative susceptibility and consequently higher levels of built-asset exposure.

The resulting Real-Estate Exposure (REE) surface is presented in Figure 16. The map illustrates the spatial coincidence between cumulative geoenvironmental susceptibility and building concentration, highlighting localized urban sectors where environmental pressures intersect with dense built development.

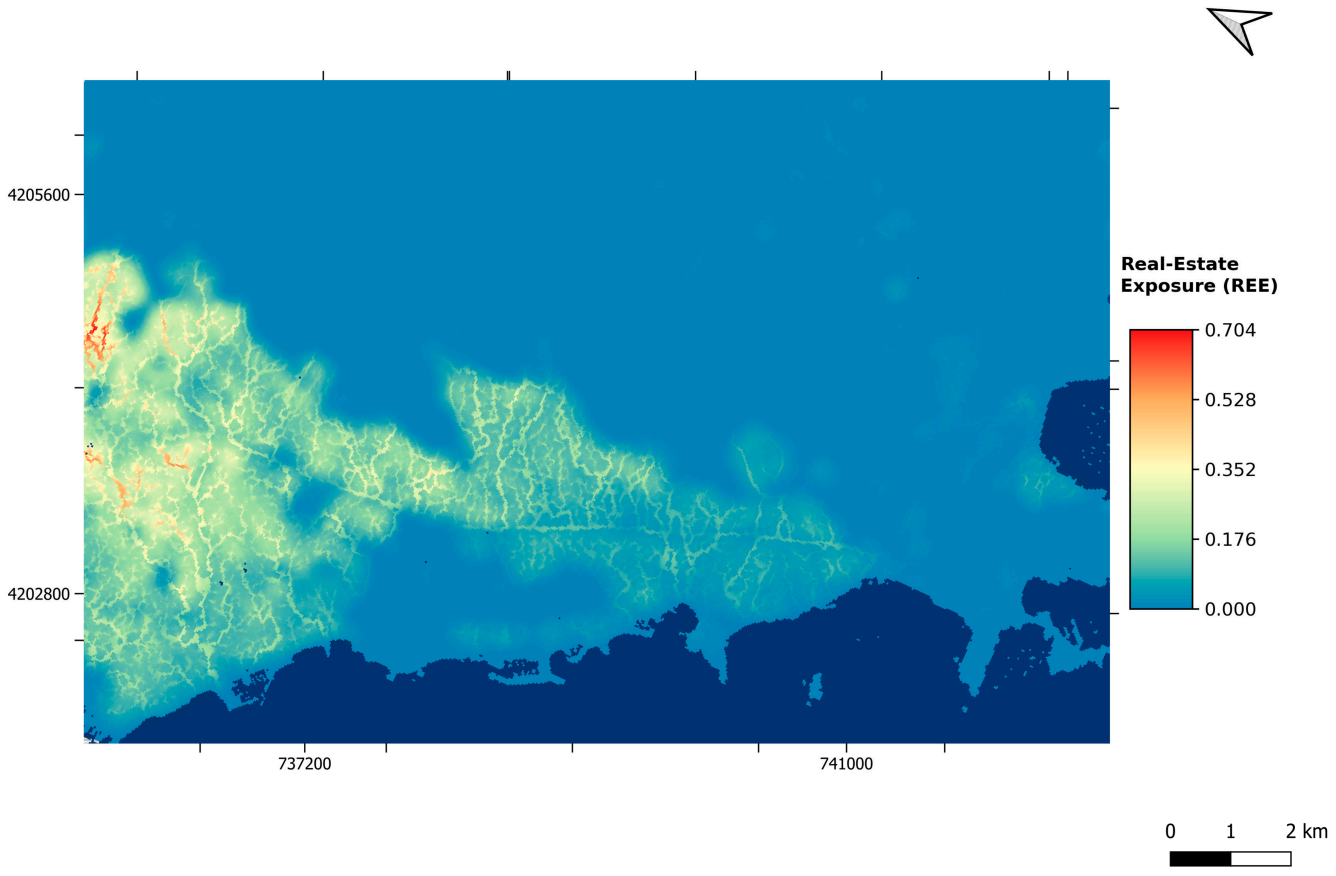


Figure 16. Spatial distribution of the Real-Estate Exposure (REE) surface obtained by combining the fuzzy-AHP Urban Geoenvironmental Impact Index (UGII) with the normalized Built-Asset Density (BAD) layer through raster multiplication. The REE surface was classified into five exposure classes (Very Low, Low, Moderate, High, and Very High) using the Natural Breaks (Jenks) classification method.

In contrast, lower exposure values are generally associated with sectors with reduced urban development intensity, greater vegetation presence, and lower building concentrations. Although some of these areas may exhibit locally elevated environmental susceptibility, the limited concentration of urban assets reduces their overall exposure significance.

Environmental susceptibility alone does not necessarily imply increased built-asset exposure. Rather, exposure emerges where susceptibility intersects with the spatial concentration of urban properties and development. This distinction highlights the importance of integrating environmental intelligence with information on the built assets when evaluating the potential implications of cumulative environmental pressures in metropolitan regions.

The resulting exposure surface is therefore a practical GIS-based decision-support product capable of supporting urban planning, redevelopment prioritization, infrastructure management, and climate adaptation strategies. By identifying sectors where multiple environmental pressures coincide with significant development concentration, the proposed framework offers a transferable approach for incorporating environmental susceptibility information into urban decision-making processes.

The statistical distribution of REE values is shown in Figure 17. The histogram exhibits a strongly positively skewed distribution, indicating that low exposure values dominate most of the metropolitan area, whereas only a limited number of cells attain high exposure values. This behaviour confirms that elevated exposure is spatially concentrated in localized hotspots rather than being uniformly distributed across the study area.

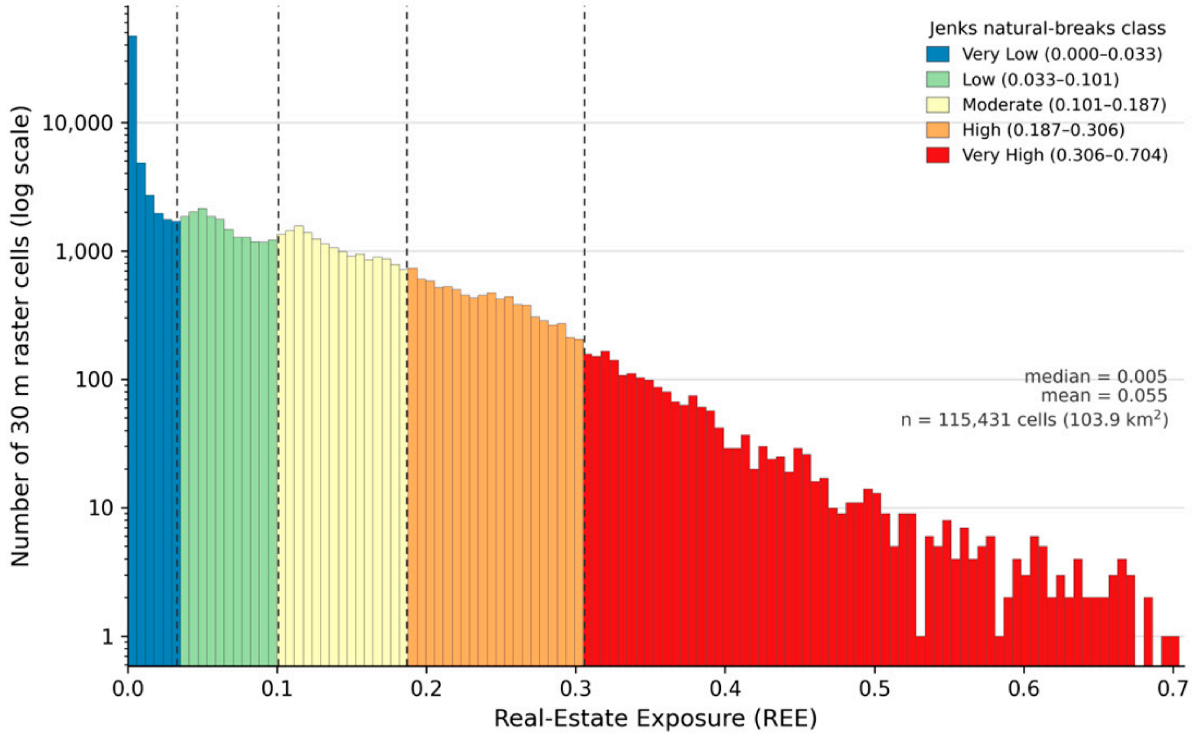


Figure 17. Histogram of Real-Estate Exposure (REE) values showing the frequency distribution of raster-cell values across the study area. The distribution is strongly positively skewed, indicating that high exposure values occupy only a limited proportion of the metropolitan area.

Table 7 summarizes the analytical progression of the proposed UGII framework from environmental indicator integration to assessing the exposure of built assets. The framework is structured as a sequential geoenvironmental process in which environmental susceptibility is first identified through conventional and fuzzy-AHP modelling and subsequently combined with building-density information. This progression enables the transition from environmental characterization to exposure-oriented spatial assessment, thereby providing information that can support urban planning, redevelopment prioritization, infrastructure resilience, and climate adaptation strategies.

Table 7. Conceptual progression of the UGII framework from susceptibility assessment to built-asset exposure interpretation.

Analytical Output	Methodological Basis	What It Represents	Main Interpretation	Planning Relevance
Conventional AHP-UGII	Linear min–max normalization + AHP weighting	Baseline cumulative urban environmental susceptibility	Is a generalized representation of the combined influence of hydrological, morphometric, thermal, vegetation, and infrastructure-related factors	Metropolitan-scale environmental screening and preliminary susceptibility assessment
Fuzzy-AHP UGII	Fuzzy membership functions + AHP weighting	Non-linear cumulative urban environmental susceptibility	Captures gradual environmental transitions, uncertainty, and non-linear responses more effectively than conventional weighted overlays	Identification of environmentally sensitive sectors and prioritization of adaptation measures
Difference Map (Fuzzy − Conventional)	Cell-by-cell subtraction of UGII surfaces	Spatial effect of fuzzy transformation	Reveals areas where fuzzy logic modifies susceptibility estimates and improves local spatial differentiation	Evaluation of methodological improvements and uncertainty representation
Built-Asset Density (BAD)	Kernel density estimation of OpenStreetMap building footprints	Spatial concentration of buildings	Represents the intensity of urban development and the distribution of potentially exposed development	Identification of development concentration patterns and urban growth hotspots
Real-Estate Exposure (REE)	Fuzzy-AHP UGII × Built-Asset Density	Spatial coincidence of environmental susceptibility and urban development	Highlights sectors where environmental pressures overlap with concentrated urban development	Supports redevelopment planning, infrastructure management, climate adaptation, and risk-informed investment decisions

The area occupied by each susceptibility class under the two formulations is summarized in Table 8.

Table 8. Area distribution of UGII susceptibility classes (Natural Breaks, Jenks) across the study area (104.3 km^2).

Class	Conventional AHP Range	Area (km^2)	%	Fuzzy-AHP Range	Area (km^2)	%
Very Low	0.175–0.308	22.9	22.0	0.102–0.301	24.8	23.8
Low	0.308–0.354	34.7	33.3	0.301–0.359	40.4	38.8
Moderate	0.354–0.410	27.1	26.0	0.359–0.440	22.9	21.9
High	0.410–0.488	13.3	12.8	0.440–0.557	9.6	9.2
Very High	0.488–0.647	6.3	6.0	0.557–0.747	6.6	6.3
Total		104.3	100		104.3	100

Note: Area values are rounded to one decimal place; therefore, totals may differ slightly from that of the reported study area (104.3 km^2) because of rounding.

The REE classification confirms that exposure is highly concentrated spatially. Approximately 61.5% of the study area belongs to the Very Low exposure class, whereas only 9.2% (High and Very High combined) exhibits elevated exposure. The Very High exposure class occupies only 1.8 km^2 (1.8% of the metropolitan area), indicating that the coincidence of high geoenvironmental susceptibility and dense built development is confined to relatively limited urban sectors. These findings demonstrate that the proposed framework identifies localized priority areas for urban resilience, redevelopment planning, infrastructure management, and climate-adaptation interventions.

Across the 104.3 km^2 study area, the conventional AHP model assigns 18.8% of the area to the High and Very High classes combined, compared with 15.5% under the fuzzy-AHP model, indicating that the elevated-susceptibility footprint is closely preserved between the two formulations. The combined Very Low and Low classes account for 55.3% of the

area under the conventional model and 62.6% under the fuzzy model, while the Moderate class contracts from 26.0% to 21.9%. Within the elevated-susceptibility range, the High class narrows from 12.8% to 9.2% while the Very High class increases marginally from 6.0% to 6.3%, indicating that fuzzy standardization slightly sharpens the distinction between the most severe susceptibility sector and the remainder of the elevated range.

Overall, the results demonstrate that the proposed UGII framework is a coherent progression from geoenvironmental characterization to susceptibility assessment and finally to built-asset exposure analysis. This sequential workflow highlights the practical value of integrating EO, fuzzy modelling, and GIS-based spatial analysis within a unified methodological framework for metropolitan environmental assessment.

Together, Figures 15–17 and Table 9 provide a complete spatial and quantitative representation of built-asset exposure across the study area.

Table 9. Area distribution of Real-Estate Exposure (REE) classes (Natural Breaks, Jenks).

Class	REE Range	Area (km^2)	%
Very Low	0.000–0.033	64.2	61.5
Low	0.033–0.101	16.2	15.6
Moderate	0.101–0.187	14.3	13.7
High	0.187–0.306	7.8	7.4
Very High	0.306–0.704	1.8	1.8
Total		104.3	100

5. Discussion

This section discusses the methodological significance and practical implications of the proposed UGII framework. Emphasis is placed on the contribution of EO-derived indicators, the role of fuzzy logic in representing cumulative urban environmental susceptibility, the comparison between conventional and fuzzy formulations, and the potential application of the resulting susceptibility and built-asset exposure surfaces in urban planning and environmental decision support.

5.1. Urban Environmental Susceptibility and the Contribution of EO-Based Indicators

The results demonstrate that cumulative urban environmental susceptibility results from the interaction of multiple environmental and anthropogenic influences rather than from any single controlling factor. The combined use of hydrological, morphometric, thermal, vegetation, and infrastructure-related indicators enabled the identification of spatial patterns that would be difficult to detect through individual-variable analysis [2,13,21].

Hydrological indicators, particularly TWI and Flow Accumulation, contributed substantially to the spatial organization of susceptibility patterns by identifying sectors characterized by enhanced runoff concentration and moisture accumulation potential [8,9]. At the same time, thermal and urban indicators, including LST, NDBI, NDVI, and Road Density, captured the influence of urbanization, infrastructure concentration, vegetation loss, and thermal stress [10,11,18,19,22]. The integration of these variables within a common analytical framework allowed the UGII to represent the multidimensional behaviour of urban geoenvironmental susceptibility.

The observed spatial patterns further confirm that environmental susceptibility within metropolitan environments is strongly influenced by the interaction between natural processes and anthropogenic landscape modification. Urban sealing, transportation infrastructure, thermal accumulation, and hydrological convergence operate simultaneously and collectively shape the functioning of urban environmental systems. Consequently, integrated EO-based approaches provide a more comprehensive representation of urban environmental conditions than single-indicator assessments [3,13].

5.2. Fuzzy Geoenvironmental Versus Conventional Weighted Overlay

The comparison between the conventional AHP-based UGII and the fuzzy-AHP formulation demonstrates that both approaches identify broadly similar susceptibility patterns across the study area. The principal hotspots remain spatially consistent, indicating that the dominant environmental controls are robust regardless of the selected standardization procedure [5].

This behaviour is consistent with previous studies comparing conventional AHP and fuzzy-AHP approaches, which similarly reported that fuzzy standardization primarily improves the spatial representation of susceptibility by refining transition zones rather than fundamentally altering the overall susceptibility pattern. However, unlike these earlier applications, which focused mainly on individual hazards such as flooding or landslides, the present framework applies fuzzy modelling to cumulative urban geoenvironmental susceptibility by integrating multiple interacting environmental and anthropogenic indicators [4,5,7].

Nevertheless, the incorporation of fuzzy membership functions modifies the representation of environmental influence by introducing gradual transitions and non-linear responses [4,6,24]. The difference analysis revealed that the most significant variations occur within intermediate susceptibility zones where environmental conditions do not clearly belong to either low- or high-susceptibility categories. Such behaviour is consistent with the inherent ambiguity of environmental information and with the gradual nature of many urban environmental processes [4,7].

The results indicate that fuzzy modelling complements conventional weighted-overlay approaches by providing a more flexible representation of environmental uncertainty and gradual spatial transitions [15]. By allowing indicator influence to vary according to degrees of membership rather than fixed proportional relationships, the fuzzy-AHP formulation provides a more realistic representation of cumulative urban environmental susceptibility [4,24]. The findings further suggest that fuzzy logic is particularly well suited to metropolitan environments where environmental processes interact continuously across space and rarely operate through clearly defined thresholds.

The comparison between the two formulations indicates that fuzzy standardization primarily refines the representation of environmental susceptibility rather than fundamentally modifying its spatial structure. Consequently, the proposed fuzzy-AHP approach should be viewed as an enhancement of conventional weighted-overlay modelling, providing a more realistic depiction of gradual environmental transitions while maintaining the overall geographical consistency of the assessment. Unlike previous fuzzy susceptibility applications that primarily address individual environmental hazards, the proposed UGII extends the fuzzy-AHP concept to a cumulative urban geoenvironmental framework by simultaneously integrating hydrological, geomorphological, thermal, ecological, and anthropogenic processes within a single transferable GIS-based methodology [4–7].

More importantly, the principal scientific contribution of the proposed UGII does not lie solely in the application of fuzzy logic, but in the development of a unified cumulative geoenvironmental assessment framework that integrates multiple interacting environmental processes within a single EO-driven methodology. By moving beyond conventional single-hazard analyses, the framework provides a transferable screening-level spatial decision-support approach capable of representing the complexity of metropolitan environmental systems through a coherent and reproducible GIS workflow.

To assess the robustness of the AHP weighting scheme, a one-at-a-time sensitivity analysis was performed, perturbing each of the nine criterion weights by ±10% and ±20% while proportionally rescaling the remaining weights to preserve unit sum. Across all 36 perturbation scenarios, the Spearman rank correlation between the perturbed and

baseline fuzzy-AHP UGII surfaces remained ≥0.990 (range 0.990–1.000), indicating that the spatial ranking of susceptibility is robust to plausible uncertainty in the expert-derived weights. The greatest sensitivity was associated with LST and R99p (ρ = 0.990–0.994 at ±20%), consistent with their comparatively high assigned weights, while Flow Accumulation, Curvature, and NDVI showed negligible sensitivity (ρ ≥ 0.9999).

5.3. Implications for Urban Planning and Built-Asset Exposure Assessment

The proposed framework has important implications for urban planning, climate adaptation, and environmental decision-making. The REE map further demonstrates that the highest exposure levels occupy only a limited proportion of the metropolitan area, indicating that priority interventions can be spatially targeted rather than uniformly distributed. The identification of sectors where multiple environmental pressures converge can support the prioritization of mitigation measures, the targeting of urban greening interventions, and the planning of drainage and resilience infrastructure. Rather than replacing detailed engineering or hydrological studies, the UGII functions as a metropolitan-scale screening-level and prioritization tool capable of identifying areas requiring further investigation [13,23].

The integration of building-density information extends the practical value of the methodology by linking environmental susceptibility with the spatial distribution of urban development. The resulting exposure assessment highlights sectors where elevated susceptibility coincides with significant concentrations of physical assets, thereby identifying locations where environmental conditions may have greater implications for urban infrastructure, redevelopment initiatives, and long-term resilience planning [2,21].

Previous GIS-based environmental assessment frameworks emphasized the importance of integrating susceptibility information into planning and infrastructure management. The present study extends this perspective by explicitly coupling cumulative geoenvironmental susceptibility with built-asset concentration, thereby providing a practical exposure-oriented decision-support layer for metropolitan environments rather than a hazard-specific assessment alone [2,13,23].

Importantly, the proposed exposure assessment should not be interpreted as a direct measure of property value or economic risk. Instead, it represents a GIS-based decision-support layer that can complement urban planning and redevelopment processes by identifying areas where cumulative environmental pressures intersect with concentrated urban development [13,15]. Because the proposed workflow relies exclusively on widely available EO data, open geospatial datasets, and transparent GIS procedures, it can be readily transferred and adapted to other metropolitan environments facing similar cumulative environmental pressures. In this context, the approach provides a foundation for incorporating environmental information into broader urban management and investment-support and urban resilience strategies.

5.4. Limitations and Future Research

Several limitations should be acknowledged. First, the analysis relies on a selected set of geoenvironmental indicators and does not explicitly incorporate socioeconomic variables, demographic characteristics, building condition, or infrastructure vulnerability. Consequently, the resulting susceptibility and exposure surfaces should be interpreted as indicators of environmental susceptibility rather than as a comprehensive urban risk assessment.

Second, the built-asset density layer was derived from OpenStreetMap building footprints and therefore depends on the completeness and positional accuracy of the available dataset. Although OpenStreetMap provides extensive coverage within the study area, variations in data quality may influence the representation of urban development intensity.

Third, the proposed exposure assessment considers the spatial concentration of built assets but does not incorporate information regarding property values, construction quality, land use, or economic activity. Future developments could integrate real-estate market indicators, cadastral information, and socioeconomic datasets to develop more comprehensive urban exposure and resilience frameworks [2,21].

The remotely sensed indicators were derived from a single Landsat 9 epoch. As only the two date-dependent indicators (LST and NDVI) carry approximately 16.3% of the aggregate weight, and as the acquisition was selected to represent peak seasonal stress, the single-epoch design is not expected to alter the principal susceptibility patterns; nevertheless, multi-temporal compositing of LST and NDVI would further reduce sensitivity to individual acquisition conditions. Further developments could explore seasonal EO composites, alternative fuzzy membership functions, machine-learning-based weighting, and dynamic monitoring systems capable of capturing changes in environmental susceptibility through time. Such developments would further enhance the applicability of the proposed methodology through support for dynamic geoenvironmental monitoring, adaptive urban planning, and climate resilience [3,8].

The parameterization of the fuzzy membership functions was not fully uniform across indicators: only the precipitation criterion (R99p) was calibrated through an explicit statistical procedure, while the remaining eight indicators were calibrated through expert interpretation of each variable's observed range. This heterogeneity in parameterization approach constitutes a methodological limitation; however, the one-at-a-time sensitivity analysis (Section 5.2) indicates that the resulting susceptibility ranking remains robust (Spearman $\rho \geq 0.990$) to substantial perturbation of the associated weights, partially mitigating this concern. Future applications could adopt a uniform, fully data-derived calibration procedure across all indicators.

Because the UGII is designed as a cumulative geoenvironmental susceptibility and decision-support framework rather than a predictive hazard model, its evaluation primarily concerns methodological consistency, weighting reliability, and the spatial coherence of the resulting susceptibility patterns. Accordingly, validation against a single hazard inventory would not provide an appropriate benchmark for the proposed framework, because the UGII does not predict individual hazard occurrence but represents the cumulative spatial propensity of urban environments to accumulate interacting environmental pressures. Independent hazard inventories are therefore considered complementary sources for future evaluation rather than mandatory validation datasets for the present methodological framework. Future applications should investigate their relationship with independent hazard inventories, observed environmental impacts, and long-term monitoring datasets across different metropolitan environments.

This evolution is consistent with the broader transition of GIS-based environmental assessment from static mapping towards dynamic EO-driven monitoring systems capable of supporting adaptive urban resilience and climate-informed spatial planning [3,13].

The resulting REE surface demonstrates that high exposure is spatially concentrated, with only a small proportion of the metropolitan area exhibiting simultaneous high environmental susceptibility and dense built development, thereby enabling the identification of priority intervention zones.

Overall, the proposed UGII framework demonstrates how EO, fuzzy logic, and GIS-based multi-criteria analysis can be integrated into a transferable methodology for assessing cumulative urban geoenvironmental susceptibility and supporting built-asset exposure assessment in metropolitan environments.

6. Conclusions

This study developed and demonstrated an Urban Geoenvironmental Impact Index (UGII) framework for the assessment of cumulative urban environmental susceptibility in the southern sector of the Athens Metropolitan Area, Greece. The proposed approach integrates EO-derived indicators, morphometric/terrain-hydrological parameters, urban infrastructure information, Analytic Hierarchy Process (AHP) weighting, and fuzzy membership functions within a unified GIS-based assessment workflow. By combining environmental and anthropogenic variables into a single spatial framework, the methodology is a transferable approach for representing cumulative urban environmental susceptibility suitable for metropolitan-scale analysis.

The results demonstrate that cumulative urban environmental susceptibility emerges from the interaction of multiple environmental and anthropogenic processes rather than from any single controlling factor. Hydrological accumulation, terrain morphology, thermal stress, vegetation distribution, urban sealing, and infrastructure concentration collectively shape the spatial patterns observed across the study area. Among the analysed variables, hydrological indicators received the highest relative importance within the weighting structure, highlighting the importance of moisture accumulation potential and runoff concentration pathways in the geoenvironmental dynamics of the metropolitan landscape.

Beyond the numerical comparison reported in Section 4, the practical implication is that fuzzy-AHP standardization offers planners a finer-grained susceptibility gradient without discarding the coarse spatial structure already familiar from conventional weighted-overlay outputs—easing adoption in planning contexts where conventional AHP mapping is already established practice.

By coupling susceptibility with building-density data, the framework moves beyond a purely biophysical assessment toward one directly actionable for redevelopment prioritization—distinguishing, for instance, high-susceptibility areas with negligible existing exposure from lower-susceptibility areas already carrying substantial built-asset concentration, a distinction conventional susceptibility mapping alone cannot make. Consequently, the proposed methodology extends beyond environmental mapping and provides a GIS-based decision-support tool capable of supporting urban planning, redevelopment prioritization, infrastructure management, and climate adaptation strategies.

The UGII is intentionally designed as a transparent and transferable methodology that can be implemented in other metropolitan environments using widely available geospatial datasets. Although the present study focuses on the Athens Metropolitan Area, the underlying methodological structure can readily be adapted to different urban contexts where environmental pressures, urban growth, and built-asset concentration interact in complex ways.

Future research should focus on expanding the spatiotemporal, hydrometeorological, and exposure dimensions of the framework through the integration of multi-temporal EO data, dynamic hydroclimatic indicators, independent environmental observation datasets, and additional information related to built assets and socioeconomic conditions. Such developments would contribute to the evolution of GIS-based geoenvironmental decision-support systems capable of supporting climate-resilient planning and risk-informed decision-making in rapidly transforming metropolitan environments.

Supplementary Materials: The following supporting information can be downloaded at https://www.mdpi.com/article/10.3390/hydrometeorology1020010/s1, Table S1. Technical parameterization of the proposed Urban Geoenvironmental Impact Index (UGII) framework.

Funding: This research received no external funding.

Institutional Review Board Statement: Not applicable.

Informed Consent Statement: Not applicable.

Data Availability Statement: The data supporting the findings of this study were obtained from publicly available sources. OpenStreetMap road-network data are openly available through the OpenStreetMap project and were extracted using the QuickOSM plugin in QGIS. ERA5-Land daily precipitation reanalysis data (1995–2024) are freely available through the Copernicus Climate Data Store (CDS). The Digital Elevation Model (DEM) used in this study was obtained from the Hellenic Cadastre. The processed geospatial datasets and derived UGII layers generated during the current study are available from the corresponding author upon reasonable request.

Acknowledgments: All scientific content, methodological decisions, data processing, analyses, interpretation of results, and conclusions were developed and verified by the author, who takes full responsibility for the content of this publication.

Conflicts of Interest: The author declares no conflicts of interest.

Abbreviations

The following abbreviations are used in this manuscript:

UGII	Urban Geoenvironmental Impact Index
EO	Earth Observation
GIS	Geographic Information System
DEM	Digital Elevation Model
NDVI	Normalized Difference Vegetation Index
NDBI	Normalized Difference Built-up Index
LST	Land Surface Temperature
TWI	Topographic Wetness Index
AHP	Analytic Hierarchy Process
CR	Consistency Ratio

References

1. Skoulidou, D.; Kazantzi, A.K. Indicator-based risk assessments for urban hazard resilience: An application for flash floods. *Environ. Hazards* **2025**, *24*, 339–364. [CrossRef]
2. Liu, S. Integrated assessment of environmental infrastructural and social risks for urban public safety. *Sci. Rep.* **2026**, *16*, 5909. [CrossRef] [PubMed]
3. Zhu, Z.; Wulder, M.A.; Roy, D.P.; Woodcock, C.E.; Hansen, M.C.; Radeloff, V.C.; Healey, S.P.; Schaaf, C.; Hostert, P.; Strobl, P.; et al. Benefits of the free and open Landsat data policy. *Remote Sens. Environ.* **2019**, *224*, 382–385. [CrossRef]
4. Feizizadeh, B.; Roodposhti, M.S.; Jankowski, P.; Blaschke, T. A GIS-based extended fuzzy multi-criteria evaluation for landslide susceptibility mapping. *Comput. Geosci.* **2014**, *73*, 208–221. [CrossRef] [PubMed]
5. Taoukidou, N.; Karpouzos, D.; Georgiou, P. Flood Hazard Assessment Through AHP, Fuzzy AHP, and Frequency Ratio Methods: A Comparative Analysis. *Water* **2025**, *17*, 2155. [CrossRef]
6. Papakonstantinou, G.F.D. Advancing Geohazard Assessment in Heritage Areas Through Fuzzy Logic. *Geographies* **2026**, *6*, 48. [CrossRef]
7. Shaikh, M.P.; Yadav, S.M.; Manekar, V.L. Flood Hazards Mapping by Linking CF, AHP, and Fuzzy Logic Techniques in Urban Areas. *Nat. Hazards Rev.* **2024**, *25*, 04023048. [CrossRef]
8. Papakonstantinou, G.F.D. Mapping Surface Water Pooling Zones and Stream Flow Accumulation Pathways for Vulnerable Populations in Athens: A Geospatial Hydrological Analysis. *Geographies* **2026**, *6*, 26. [CrossRef]
9. Beven, K.J.; Kirkby, M.J. A physically based, variable contributing area model of basin hydrology. *Hydrol. Sci. Bull.* **1979**, *24*, 43–69. [CrossRef]
10. Zha, Y.; Gao, J.; Ni, S. Use of normalized difference built-up index in automatically mapping urban areas from TM imagery. *Int. J. Remote Sens.* **2003**, *24*, 583–594. [CrossRef]
11. Tucker, C.J. Red and photographic infrared linear combinations for monitoring vegetation. *Remote Sens. Environ.* **1979**, *8*, 127–150. [CrossRef]
12. Papakonstantinou, G.F.D. Identifying Extreme Heat and Moisture Zones for Vulnerable Populations in Athens: A Geospatial Analysis. *Land* **2025**, *14*, 1375. [CrossRef]

13. Hawchar, L.; Naughton, O.; Nolan, P.; Stewart, M.G.; Ryan, P.C. A GIS-based framework for high-level climate change risk assessment of critical infrastructure. *Clim. Risk Manag.* **2020**, *29*, 100235. [CrossRef]
14. Wu, C.; Shui, W.; Huang, Z.; Wang, C.; Wu, Y.; Wu, Y.; Xue, C.; Huang, Y.; Zhang, Y.; Zheng, D. Urban heat vulnerability: A dynamic assessment using multi-source data in coastal metropolis of Southeast China. *Front. Public Health* **2022**, *10*, 989963. [CrossRef] [PubMed]
15. Malczewski, J. GIS-based multicriteria decision analysis: A survey of the literature. *Int. J. Geogr. Inf. Sci.* **2006**, *20*, 703–726. [CrossRef]
16. Papakonstantinou, G.F.D.; Papadopoulou, M.P. Geohazard Prevention Framework: Introducing a Cumulative Index in the Context of Management and Protection of Cultural and Natural Heritage Areas. *Land* **2024**, *13*, 1239. [CrossRef]
17. Pimenta, L.; Duarte, L.; Teodoro, A.C.; Beltrão, N.; Gomes, D.; Oliveira, R. GIS-Based Flood Susceptibility Mapping Using AHP in the Urban Amazon: A Case Study of Ananindeua, Brazil. *Land* **2025**, *14*, 1543. [CrossRef]
18. Cetin, M.; Kavlak, O.M.; Kurkcuoglu, M.A.S.; Ozturk, G.B.; Cabuk, S.N.; Cabuk, A. Determination of land surface temperature and urban heat island effects with remote sensing capabilities: The case of Kayseri, Türkiye. *Nat. Hazards* **2024**, *120*, 5509–5536. [CrossRef]
19. Altıner, F.; Bingöl, F. Spatio-Temporal Assessment of Land Surface Temperature, Vegetation Cover, and Built-Up Areas Using LST, NDVI, and NDBI in Balıkesir, Türkiye. *Sustainability* **2025**, *17*, 9245. [CrossRef]
20. Intergovernmental Panel on Climate Change (IPCC). Mediterranean Region. In *Climate Change 2022—Impacts, Adaptation and Vulnerability: Working Group II Contribution to the Sixth Assessment Report of the Intergovernmental Panel on Climate Change*; Pörtner, H.-O., Roberts, D.C., Tignor, M., Poloczanska, E.S., Mintenbeck, K., Alegría, A., Craig, M., Langsdorf, S., Löschke, S., Möller, V., et al., Eds.; Cambridge University Press: Cambridge, UK, 2023; pp. 2233–2272. [CrossRef]
21. Sohn, W.; Xu, Z.; Lu, G.; Kim, J.H. An integrated vulnerability-resilience framework for climate risk assessment in depopulating urban landscapes. *Landsc. Urban Plan.* **2026**, *271*, 105620. [CrossRef]
22. Roba, Z.R.; Tabor, K.W. Geospatial analysis of vegetation and land surface temperature for urban heat island mitigation in Hawassa City, Ethiopia. *Sci. Rep.* **2025**, *15*, 31786. [CrossRef] [PubMed]
23. Mascheri, G.; Chieffo, N.; Arrighi, C.; Del Gaudio, C.; Lourenco, P.B. A framework for multi-risk assessment in a historical area of Lisbon. *Int. J. Disaster Risk Reduct.* **2024**, *108*, 104508. [CrossRef]
24. Zadeh, L.A. Fuzzy Sets. *Inf. Control* **1965**, *8*, 338–353. [CrossRef]
25. Panagiotou, C.F.; Feloni, E.; Aristidou, K.; Eliades, M. Probabilistic Assessment of Flood Susceptibility via a Coparticipative Multicriteria Decision Analysis. *Environ. Process.* **2025**, *12*, 22. [CrossRef]
26. Dilalos, S.; Alexopoulos, J.D. The contribution of an urban gravity survey to the determinable perspective of Athens city (Greece) underground structure. *SN Appl. Sci.* **2020**, *2*, 1797. [CrossRef]
27. Papanikolaou, D.; Kranis, H.; Bassi, E.K.; Danamos, G. Paleogeographic evolution of the Athens basin from Upper Miocene to present. In Proceedings of the 10th International Congress of the Geological Society of Greece, Thessaloniki, Greece, 15–17 April 2004; Volume 36. [CrossRef]
28. Peel, M.C.; Finlayson, B.L.; Mcmahon, T. Updated World Map of the Köppen-Geiger Climate Classification. *Hydrol. Earth Syst. Sci.* **2007**, *11*, 1633–1644. [CrossRef]
29. Lionello, P.; Scarascia, L. The relation between climate change in the Mediterranean region and global warming. *Reg. Environ. Change* **2018**, *18*, 1481–1493. [CrossRef]
30. Giorgi, F. Climate change Hot-Spots. *Geophys. Res. Lett.* **2006**, *33*, L08707. [CrossRef]
31. Muñoz-Sabater, J.; Dutra, E.; Agustí-Panareda, A.; Albergel, C.; Arduini, G.; Balsamo, G.; Boussetta, S.; Choulga, M.; Harrigan, S.; Hersbach, H.; et al. ERA5-Land: A State-of-the-Art Global Reanalysis Dataset for Land Applications. *Earth Syst. Sci. Data* **2021**, *13*, 4349–4383. [CrossRef]
32. Zhang, X.; Alexander, L.; Hegerl, G.C.; Jones, P.; Tank, A.K.; Peterson, T.C.; Trewin, B.; Zwiers, F.W. Indices for monitoring changes in extremes based on daily temperature and precipitation data. *WIREs Clim. Change* **2011**, *2*, 851–870. [CrossRef]
33. Saaty, T.L. *The Analytic Hierarchy Process*; McGraw-Hill: New York, NY, USA, 1980.
34. Saaty, T.L. A scaling method for priorities in hierarchical structures. *J. Math. Psychol.* **1977**, *15*, 234–281. [CrossRef]
35. Jenks, G.F. Generalization in Statistical Mapping. *Ann. Assoc. Am. Geogr.* **1963**, *53*, 15–26. [CrossRef]

Disclaimer/Publisher's Note: The statements, opinions and data contained in all publications are solely those of the individual author(s) and contributor(s) and not of MDPI and/or the editor(s). MDPI and/or the editor(s) disclaim responsibility for any injury to people or property resulting from any ideas, methods, instructions or products referred to in the content.